Chapter 7
Hybrid Simulation Methods: Combining Finite Element Methods and Analytical Solutions

S. Duczek, Z.A.B. Ahmad, J.M. Vivar-Perez, and U. Gabbert

Abstract In the context of wave propagation analysis the computational efficiency of numerical and semi-analytical methods is essential, as very fine spatial and temporal resolutions are required in order to describe all phenomena of interest, including scattering, reflection, mode conversion, and many more. These strict demands originate from the fact that high-frequency ultrasonic guided waves are investigated. In this chapter, our focus is on developing semi-analytical methods based on higher order basis functions and demonstrating their range of applicability. Thereby, we discuss the semi-analytical finite element method (SAFE) and a hybrid approach coupling spectral elements with analytical solutions in the frequency domain. The results illustrate that higher order methods are essential in order to decrease the numerical costs. Moreover, it is demonstrated that the proposed approaches are the methods of choice when we want to compute dispersion diagrams or if large parts of the structure are undisturbed and, therefore, can be described by analytical solutions. If, however, complex geometries are considered or the whole structure has to be investigated, only purely FE-based approaches seem to be a viable option.

7.1 The Semi-Analytical Finite Element Method

The content of the current section is primarily based on Dr. Ahmad's research. The results of his investigations are published in a PhD thesis [1] and in two peer-reviewed journal articles [2, 3].

The semi-analytical finite element method (SAFE) is typically used to compute the dispersion curves for isotropic and composite plates [1]. More complex waveguides, such as rods, wires, and rail road tracks, have also been investigated [4, 9, 15, 27, 38, 44, 53]. If we want to consider the effect of initial axial loads on the dispersion curves, additional terms need to be added to the conventional formulation [43]. As in standard FE applications, both *h*- and/or *p*-refinements

S. Duczek (✉) • Z.A.B. Ahmad • J.M. Vivar-Perez • U. Gabbert (✉)
Institute of Mechanics, Otto von Guericke University Magdeburg, Universitätsplatz 2, 39106 Magdeburg, Germany
e-mail: sascha.duczek@ovgu.de; ulrich.gabbert@ovgu.de

R. Lammering et al. (eds.), *Lamb-Wave Based Structural Health Monitoring in Polymer Composites*, Research Topics in Aerospace,
DOI 10.1007/978-3-319-49715-0_7

can be deployed to increase the accuracy of the simulations. This is especially important when higher order wave modes need to be evaluated [8]. The influence of external loads and a piezoelectric excitation can also be included in the SAFE formulation. For two-dimensional problems this is discussed in [9, 48] and three-dimensional (3D) cases are considered in [7, 57]. These simulations solve the wave propagation problem for plates with infinite (in-plane) dimensions, due to the fact that the SAFE method implicitly assumes the plate to be infinite in its formulation. Additional effects on the propagation of elastic guided waves, i.e. reflections and transmissions from damages, actuators or boundaries make the wave propagation behavior more complex and must be added separately. Therefore, the SAFE method can be combined with classical methods, such as the FEM, the boundary element method (BEM), and other computational approaches. The reflection and transmission behavior of ultrasonic guided waves at geometrical perturbations of the infinite plate have been investigated in [2, 3, 23, 35, 36, 39, 54, 55]. In these cases, the infinite plate section is modeled using the SAFE approach, while damages or boundaries are modeled using the FEM or the BEM, respectively [2, 3]. Leaky Lamb waves are also investigated with the help of SAFE to evaluate the energy loss into the surrounding medium [24, 29, 46].

7.1.1 Motivation

The SAFE method has its advantages in the computation of dispersion curves and in the analysis of wave interactions with obstacles. The solution to both problems benefits from the semi-analytical character of the SAFE. That is to say, unperturbed regions of a structure or infinite regions can be simulated at hardly any cost compared to classical FE approaches. The SAFE is not as severely affected by the need for a fine spatial discretization compared to the FEM because of its specifically tailored basis functions that account for typical properties of propagating waves. The details behind this behavior are explained in Sects. 7.1.2–7.1.6.

7.1.2 Theoretical Principles

In this section we provide the formulation of the semi-analytical finite element method according to [4, 13–15, 41, 45]. The SAFE method is basically a combination of the FEM in the cross section of the structure and analytical methods in the direction of wave propagation direction. Accordingly, we discretize the cross section of the waveguide by means of conventional finite elements and deploy a complex exponential function in the propagation direction [14], cf. Fig. 7.1. That is to say, we reduce the dimensionality of the problem by one which is also the reason for the decreased computational costs. Since the plate thickness can easily be resolved by only a few finite elements mesh requirements for the SAFE method are

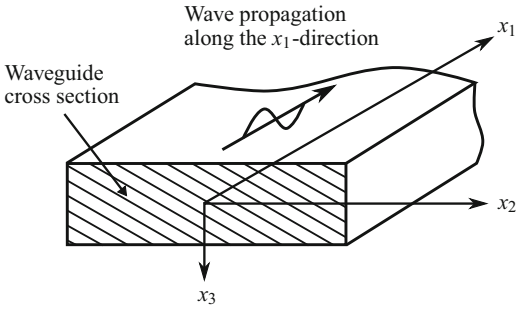

Fig. 7.1 Sketch of the cross section of a plate-like waveguide

comparably low [1]. In the remainder of this chapter we will use the term in-plane to refer to the cross section plane of the waveguide, while out-of-plane denotes the wave propagation direction, cf. Fig. 7.1. Note that this is in contrast to the natural understanding of the words in- and out-of-plane.

The point of departure for the derivation of the SAFE is the weak form of the equilibrium equations as discussed in Chap. 4. For the sake of clarity and simplicity, we only repeat the weak form of the mechanical equilibrium equations at this point

$$\int_{\Omega} \mathbf{v}_{\mathrm{u}}^{T} \rho \ddot{\mathbf{u}} \mathrm{d}\Omega + \int_{\Omega} (\nabla_{\mathrm{u}} \mathbf{v}_{\mathrm{u}})^{T} \mathbf{C} \nabla_{\mathrm{u}} \mathbf{u} \mathrm{d}\Omega - \int_{\Omega} \mathbf{v}_{\mathrm{u}}^{T} \mathbf{b} \mathrm{d}\Omega - \int_{\Gamma_{\mathrm{u}}} \mathbf{v}_{\mathrm{u}}^{T} \bar{\mathbf{t}} \mathrm{d}\Gamma = 0 \,, \tag{7.1}$$

with Ω and Γ denoting the computational domain and its boundary. The loading of the structure is given by $\mathbf{b}$ and $\mathbf{t}$ which are the vector of body forces and the surface traction vector, respectively. The overbar represents a prescribed value at the Neumann boundary. The mechanical displacement field is denoted by $\mathbf{u}$ and the test functions corresponding to the method of weighted residuals are $\mathbf{v}_{\mathrm{u}}$. The material properties are given by $\mathbf{C}$, the elasticity matrix, and by ρ, the mass density. In the framework of the SAFE we split the mechanical differential operator matrix ∇_{u} into three parts to separate the derivatives with respect to the individual coordinates [45] as

$$\nabla_{\mathrm{u}} = \begin{bmatrix} \frac{\partial}{\partial x_1} & 0 & 0 & \frac{\partial}{\partial x_2} & 0 & \frac{\partial}{\partial x_3} \\ 0 & \frac{\partial}{\partial x_2} & 0 & \frac{\partial}{\partial x_1} & \frac{\partial}{\partial x_3} & 0 \\ 0 & 0 & \frac{\partial}{\partial x_3} & 0 & \frac{\partial}{\partial x_2} & \frac{\partial}{\partial x_1} \end{bmatrix}^{T} = \mathbf{L}_{x_1} \frac{\partial}{\partial x_1} + \mathbf{L}_{x_2} \frac{\partial}{\partial x_2} + \mathbf{L}_{x_3} \frac{\partial}{\partial x_3} \,, \tag{7.2}$$

with

$$\mathbf{L}_{x_1} = \begin{bmatrix} 1\,0\,0 \\ 0\,0\,0 \\ 0\,0\,0 \\ 0\,0\,0 \\ 0\,0\,1 \\ 0\,1\,0 \end{bmatrix}, \quad \mathbf{L}_{x_2} = \begin{bmatrix} 0\,0\,0 \\ 0\,1\,0 \\ 0\,0\,0 \\ 0\,0\,1 \\ 0\,0\,0 \\ 1\,0\,0 \end{bmatrix}, \quad \mathbf{L}_{x_3} = \begin{bmatrix} 0\,0\,0 \\ 0\,0\,0 \\ 0\,0\,1 \\ 0\,1\,0 \\ 1\,0\,0 \\ 0\,0\,0 \end{bmatrix}.$$

In the next step we discretize the displacement field in a similar fashion as known from the FEM. In the framework of the SAFE we assume that the displacement field is a harmonic function in x_1 and the cross section ($x_2 - x_3$ plane) of the plate is discretized by conventional two-dimensional finite elements. Therefore, we can express the displacement vector as [4]

$$\mathbf{u}(\mathbf{x}, t) = \tilde{\mathbf{N}}(x_2, x_3)\mathbf{U}_\mathrm{e} \mathrm{e}^{-j(kx_1 - \omega t)}\,, \tag{7.3}$$

where $j = \sqrt{-1}$ represents the imaginary unit and $\tilde{\mathbf{N}}(x_2, x_3)$ is the two-dimensional basis function matrix. The wavenumber and the circular frequency are denoted by k and ω, respectively. Keep in mind that we use the same ansatz also for the test functions $\mathbf{v}_\mathrm{u}$

$$\mathbf{v}_\mathrm{u}(\mathbf{x}, t) = \tilde{\mathbf{N}}(x_2, x_3)\mathbf{V}_\mathrm{ue} \mathrm{e}^{-j(kx_1 - \omega t)}\,. \tag{7.4}$$

The basis function matrix $\tilde{\mathbf{N}}$ and the vector of nodal degrees of freedom $\mathbf{U}_\mathrm{e}$ have the following form

$$\tilde{\mathbf{N}} = \begin{bmatrix} N^{\mathrm{N}_1} & & & N^{\mathrm{N}_2} & & & & N^{\mathrm{N}_{n_\mathrm{Node}}} & \\ & N^{\mathrm{N}_1} & & & N^{\mathrm{N}_2} & & \dots & & N^{\mathrm{N}_{n_\mathrm{Node}}} \\ & & N^{\mathrm{N}_1} & & & N^{\mathrm{N}_2} & & & N^{\mathrm{N}_{n_\mathrm{Node}}} \end{bmatrix}, \tag{7.5}$$

$$\mathbf{U}_\mathrm{e} = \begin{bmatrix} u_1^{\mathrm{N}_1} & u_2^{\mathrm{N}_1} & u_3^{\mathrm{N}_1} & u_1^{\mathrm{N}_2} & u_2^{\mathrm{N}_2} & u_3^{\mathrm{N}_2} & \dots & u_1^{\mathrm{N}_{n_\mathrm{Node}}} & u_2^{\mathrm{N}_{n_\mathrm{Node}}} & u_3^{\mathrm{N}_{n_\mathrm{Node}}} \end{bmatrix}^T, \tag{7.6}$$

where n_Node is the number of nodes per finite element. At this point we also introduce the linear strain–displacement relation

$$\boldsymbol{\varepsilon}_\mathrm{u} = \nabla_\mathrm{u}\mathbf{u}\,. \tag{7.7}$$

If we now substitute Eqs. (7.2) and (7.3) into Eq. (7.7), we obtain [45]

$$\boldsymbol{\varepsilon}_\mathrm{u} = \left(\mathbf{B}_\mathrm{u}^* - jk\mathbf{B}_\mathrm{u}^\#\right)\mathbf{U}_\mathrm{e} \mathrm{e}^{-j(kx_1 - \omega t)} \tag{7.8}$$

with

$$\mathbf{B}_{\mathrm{u}}^{*} = \mathbf{L}_{x_2}\tilde{\mathbf{N}}_{,x_2} + \mathbf{L}_{x_3}\tilde{\mathbf{N}}_{,x_3} \,, \tag{7.9}$$

$$\mathbf{B}_{\mathrm{u}}^{\#} = \mathbf{L}_{x_1}\tilde{\mathbf{N}} \,. \tag{7.10}$$

The derivatives with respect to the variables x_i are denoted by $(\cdot)_{,x_i}$. The semi-discrete equations of motion for one element can be derived from Eq. (7.1) and are given as

$$\begin{aligned}
&\int_{\Omega_{\mathrm{e}}} \left[\tilde{\mathbf{N}}(x_2,x_3)\mathbf{V}_{\mathrm{ue}}\mathrm{e}^{-j(kx_1-\omega t)}\right]^T \rho\, \frac{\partial^2}{\partial t^2}\left[\tilde{\mathbf{N}}(x_2,x_3)\mathbf{U}_{\mathrm{e}}\mathrm{e}^{-j(kx_1-\omega t)}\right] \mathrm{d}\Omega + \\
&\int_{\Omega_{\mathrm{e}}} \left[\left(\mathbf{B}_{\mathrm{u}}^{*} - jk\mathbf{B}_{\mathrm{u}}^{\#}\right)\mathbf{V}_{\mathrm{ue}}\mathrm{e}^{-j(kx_1-\omega t)}\right]^T \mathbf{C}\left[\left(\mathbf{B}_{\mathrm{u}}^{*} - jk\mathbf{B}_{\mathrm{u}}^{\#}\right)\mathbf{U}_{\mathrm{e}}\mathrm{e}^{-j(kx_1-\omega t)}\right] \mathrm{d}\Omega - \\
&\int_{\Omega_{\mathrm{e}}} \left[\tilde{\mathbf{N}}(x_2,x_3)\mathbf{V}_{\mathrm{ue}}\mathrm{e}^{-j(kx_1-\omega t)}\right]^T \mathbf{b}\,\mathrm{d}\Omega - \\
&\int_{\Gamma_{\mathrm{u}}^{\mathrm{e}}} \left[\tilde{\mathbf{N}}(x_2,x_3)\mathbf{V}_{\mathrm{ue}}\mathrm{e}^{-j(kx_1-\omega t)}\right]^T \bar{\mathbf{t}}\,\mathrm{d}\Gamma = 0 \,.
\end{aligned} \tag{7.11}$$

In the next steps we simplify the first two terms of Eq. (7.11) and derive the stiffness matrix $\mathbf{K}_{\mathrm{u}}$ and the mass matrix $\mathbf{M}_{\mathrm{u}}$ corresponding to the semi-analytical finite element method. The ansatz for the displacement field and the test functions has the inherent advantage that we can easily split the domain integration into two separate parts. First, we solve the one-dimensional integral with respect to x_1 and then we perform a domain integration over the $x_2 - x_3$ plane denoted by $\Omega^{\times}$ [4]. In order to transpose a complex matrix we need to compute the conjugate transpose matrix by negating the imaginary part. Therefore the first two terms in Eq. (7.11) are given by

$$\begin{aligned}
&\int_{\Omega_{\mathrm{e}}} \left[\tilde{\mathbf{N}}(x_2,x_3)\mathbf{V}_{\mathrm{ue}}\mathrm{e}^{-j(kx_1-\omega t)}\right]^T \rho\, \frac{\partial^2}{\partial t^2}\left[\tilde{\mathbf{N}}(x_2,x_3)\mathbf{U}_{\mathrm{e}}\mathrm{e}^{-j(kx_1-\omega t)}\right] \mathrm{d}\Omega = \\
&\int_{\Omega_{\mathrm{e}}^{\times}} \int_{x_1} -\omega^2\rho \left[\mathbf{V}_{\mathrm{ue}}^T\tilde{\mathbf{N}}(x_2,x_3)^T\tilde{\mathbf{N}}(x_2,x_3)\mathbf{U}_{\mathrm{e}}\right] \mathrm{d}\,x_1\mathrm{d}\Omega^{\times} = \\
&-\omega^2 x_1 \mathbf{V}_{\mathrm{ue}}^T \int_{\Omega_{\mathrm{e}}^{\times}} \rho \left[\tilde{\mathbf{N}}(x_2,x_3)^T\tilde{\mathbf{N}}(x_2,x_3)\right] \mathrm{d}\Omega^{\times}\mathbf{U}_{\mathrm{e}} \,,
\end{aligned} \tag{7.12}$$

$$\begin{aligned}
&\int_{\Omega_{\mathrm{e}}} \left[\left(\mathbf{B}_{\mathrm{u}}^{*} - jk\mathbf{B}_{\mathrm{u}}^{\#}\right)\mathbf{V}_{\mathrm{ue}}\mathrm{e}^{-j(kx_1-\omega t)}\right]^T \mathbf{C}\left[\left(\mathbf{B}_{\mathrm{u}}^{*} - jk\mathbf{B}_{\mathrm{u}}^{\#}\right)\mathbf{U}_{\mathrm{e}}\mathrm{e}^{-j(kx_1-\omega t)}\right] \mathrm{d}\Omega = \\
&\int_{\Omega_{\mathrm{e}}^{\times}} \int_{x_1} \mathbf{V}_{\mathrm{ue}}^T \left[\mathbf{B}_{\mathrm{u}}^{*T} + jk\mathbf{B}_{\mathrm{u}}^{\#T}\right] \mathbf{C}\left[\mathbf{B}_{\mathrm{u}}^{*} - jk\mathbf{B}_{\mathrm{u}}^{\#}\right] \mathbf{U}_{\mathrm{e}}\mathrm{d}\,x_1\mathrm{d}\Omega^{\times} = \\
&x_1\mathbf{V}_{\mathrm{ue}}^T \int_{\Omega_{\mathrm{e}}^{\times}} \left[\mathbf{B}_{\mathrm{u}}^{*T}\mathbf{C}\mathbf{B}_{\mathrm{u}}^{*} + jk\mathbf{B}_{\mathrm{u}}^{\#T}\mathbf{C}\mathbf{B}_{\mathrm{u}}^{*} - jk\mathbf{B}_{\mathrm{u}}^{*T}\mathbf{C}\mathbf{B}_{\mathrm{u}}^{\#} + k^2\mathbf{B}_{\mathrm{u}}^{\#T}\mathbf{C}\mathbf{B}_{\mathrm{u}}^{\#}\right] \mathrm{d}\Omega^{\times}\mathbf{U}_{\mathrm{e}} \,.
\end{aligned} \tag{7.13}$$

As mentioned before Eq. (7.11) represents the contribution of one finite element to the weak from. Therefore, we have to sum the contributions of all n_{el} elements to obtain the semi-discrete (homogeneous) equations of motion for the system under investigation as

$$\sum_{e=1}^{n_{\mathrm{el}}} \left[\mathbf{K}^{\mathrm{e}}_{11\mathrm{u}} + jk\mathbf{K}^{\mathrm{e}}_{12\mathrm{u}} + k^2\mathbf{K}^{\mathrm{e}}_{22\mathrm{u}} - \omega^2\mathbf{M}^{\mathrm{e}}_{\mathrm{u}}\right]\mathbf{U}_{\mathrm{e}} = \mathbf{0}\,, \tag{7.14}$$

where $\mathbf{K}^{\mathrm{e}}_{11\mathrm{u}}$, $\mathbf{K}^{\mathrm{e}}_{12\mathrm{u}}$, $\mathbf{K}^{\mathrm{e}}_{22\mathrm{u}}$, and $\mathbf{M}^{\mathrm{e}}_{\mathrm{u}}$ denote the in-plane stiffness matrix, the coupling stiffness matrix, the out-of-plane stiffness matrix, and the mass matrix, respectively. Their definitions are given below

$$\mathbf{K}^{\mathrm{e}}_{11\mathrm{u}} = \int_{\Omega^{\times}_{\mathrm{e}}} \mathbf{B}^{*T}_{\mathrm{u}}\mathbf{C}\mathbf{B}^{*}_{\mathrm{u}}\,\mathrm{d}\Omega^{\times}\,, \tag{7.15}$$

$$\mathbf{K}^{\mathrm{e}}_{12\mathrm{u}} = \int_{\Omega^{\times}_{\mathrm{e}}} \mathbf{B}^{\#T}_{\mathrm{u}}\mathbf{C}\mathbf{B}^{*}_{\mathrm{u}}\,\mathrm{d}\Omega^{\times} - \int_{\Omega^{\times}_{\mathrm{e}}} \mathbf{B}^{*T}_{\mathrm{u}}\mathbf{C}\mathbf{B}^{\#}_{\mathrm{u}}\,\mathrm{d}\Omega^{\times}\,, \tag{7.16}$$

$$\mathbf{K}^{\mathrm{e}}_{22\mathrm{u}} = \int_{\Omega^{\times}_{\mathrm{e}}} \mathbf{B}^{\#T}_{\mathrm{u}}\mathbf{C}\mathbf{B}^{\#}_{\mathrm{u}}\,\mathrm{d}\Omega^{\times}, \tag{7.17}$$

$$\mathbf{M}^{\mathrm{e}}_{\mathrm{u}} = \int_{\Omega^{\times}_{\mathrm{e}}} \rho\tilde{\mathbf{N}}^{*T}\tilde{\mathbf{N}}\,\mathrm{d}\Omega^{\times}\,. \tag{7.18}$$

Equation (7.14) constitutes the eigenvalue problem of the SAFE method which has to be solved to compute the propagation of elastic guided waves in infinite media. For further information on the SAFE method, the interested reader is referred to [22, 23, 26, 27, 32–37, 39, 40, 50] and the references cited therein.

7.1.3 Plate with Infinite Dimensions

Considering a plate with infinite dimensions in x_1- and x_2-directions we can further simplify the SAFE equations as there is no dependence of the displacement field on x_2 [45]. Therefore, only the thickness of the plate has to be discretized by one-dimensional finite elements. This is illustrated in Fig. 7.2. Due to this simplification the strain–displacement relation is given by

$$\boldsymbol{\varepsilon}_{\mathrm{u}} = \left(\mathbf{B}^{*}_{\mathrm{u}} - jk\mathbf{B}^{\#}_{\mathrm{u}}\right)\mathbf{U}_{\mathrm{e}}\mathrm{e}^{-j(kx_1-\omega t)} \tag{7.19}$$

with

$$\mathbf{B}^{*}_{\mathrm{u}} = \mathbf{L}_{x_3}\tilde{\mathbf{N}}_{,x_3}\,, \tag{7.20}$$

$$\mathbf{B}^{\#}_{\mathrm{u}} = \mathbf{L}_{x_1}\tilde{\mathbf{N}}\,. \tag{7.21}$$

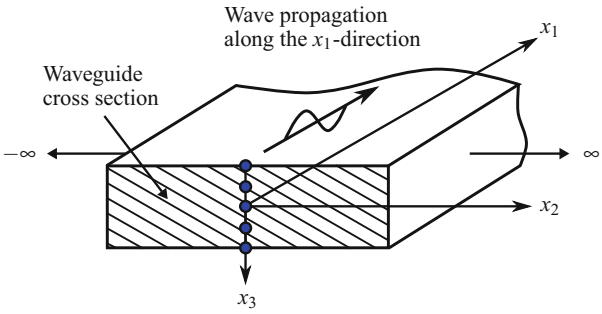

Fig. 7.2 Sketch of the cross section of an infinite plate. The finite element discretization is indicated by its nodes (one-dimensional elements)

This also implies that the integration domain changes from $\mathrm{d}\Omega^{\times}$ to $\mathrm{d}\,x_3$. The integrals in Eqs. (7.15)–(7.18) can now be evaluated numerically by a standard one-dimensional Gaussian quadrature rule.

In the context of the FEM it is advantageous to define the basis functions with respect to a reference domain [11, 28, 66]. Therefore, the finite elements need to be mapped from the reference frame to the global domain as discussed in Sect. 4.7. This procedure is exemplarily discussed for a 3-noded (quadratic) isoparametric finite element. The basis functions are [66]

$$N_{\mathrm{u},3}^{\mathrm{N}_1}(\xi_1) = \frac{1}{2}\xi_1(\xi_1 - 1)\,, \tag{7.22}$$

$$N_{\mathrm{u},3}^{\mathrm{N}_2}(\xi_1) = (1 - \xi_1^2)\,, \tag{7.23}$$

$$N_{\mathrm{u},3}^{\mathrm{N}_3}(\xi_1) = \frac{1}{2}\xi_1(\xi_1 + 1)\,. \tag{7.24}$$

For the infinite plate the domain integration over the cross section is simply given by

$$\int_{\Omega_e^{\times}} \ldots \mathrm{d}\Omega = \int_{\xi_3=-1}^{1} \ldots \det(\mathbf{J})\mathrm{d}\xi_3\,, \tag{7.25}$$

where $\mathbf{J}$ denotes the Jacobian matrix of the mapping. In the one-dimensional case the evaluation of Eq. (4.59) reduces to a scalar value

$$J = \frac{\mathrm{d}\,x_3}{\mathrm{d}\xi_1}\,. \tag{7.26}$$

Due to the isoparametric mapping concept discussed in Sect. 4.7.2 we can express x_3 within an element by a linear combination of the basis functions and the nodal coordinates X_3^i by

$$x_3 = \mathrm{Q}^{(\mathrm{e})}(\xi_1) = \sum_{i=1}^{3} N_{\mathrm{u},3}^{\mathrm{N}_i}(\xi_1) X_3^i \,. \tag{7.27}$$

With the help of Eq. (7.27) we can compute the Jacobian matrix in terms of the nodal coordinates and the local coordinate ξ_1

$$J = \sum_{i=1}^{3} \frac{\mathrm{d}N_{\mathrm{u},3}^{\mathrm{N_i}}(\xi_1)}{\mathrm{d}\xi_1} X_3^i = \begin{bmatrix} \xi_1 - 1 & -2\xi_1 & \xi_1 + 1 \end{bmatrix} \begin{bmatrix} X_3^1 \\ X_3^2 \\ X_3^3 \end{bmatrix} \,. \tag{7.28}$$

7.1.4 Dispersion Curves for Undamped Media

When studying the propagation of elastic guided waves the knowledge of the group and phase velocity dispersion diagrams is essential. These curves provide information on the number of propagating modes for a specific combination of excitation frequency and plate thickness and naturally on the wave velocities of these wave modes. Therefore, we need to solve the SAFE eigenvalue problem formulated in Eq. (7.14). From the definition of the system matrices provided in Eqs. (7.15)–(7.18) we know that $\mathbf{K}_{11\mathrm{u}}$, $\mathbf{K}_{22\mathrm{u}}$, and $\mathbf{M}_{\mathrm{u}}$ are symmetric matrices, while $\mathbf{K}_{12\mathrm{u}}$ is skew-symmetric [1].

Without loss of generality, we introduce a transformation matrix $\mathbf{T}$ to eliminate the imaginary unit in Eq. (7.14). To this end, we premultiply Eq. (7.14) by the transpose of $\mathbf{T}$ [4]

$$\mathbf{T}^T \left[\mathbf{K}_{11\mathrm{u}} + jk\mathbf{K}_{12\mathrm{u}} + k^2\mathbf{K}_{22\mathrm{u}} - \omega^2\mathbf{M}_{\mathrm{u}} \right] \mathbf{U} = \mathbf{0} \,. \tag{7.29}$$

The transformation matrix is a $(n_{\mathrm{dof}} \times n_{\mathrm{dof}})$-diagonal matrix which is equal to 1 at the rows corresponding to displacements in x_2- and x_3-direction and equal to the imaginary unit j at those rows corresponding to displacements in x_1 direction

$$\mathbf{T} = \begin{bmatrix} j & & & & & & \\ & 1 & & & \mathbf{0} & & \\ & & 1 & & & & \\ & & & \ddots & & & \\ & & & & j & & \\ & \mathbf{0} & & & & 1 & \\ & & & & & & 1 \end{bmatrix} \,. \tag{7.30}$$

This matrix has some favorable properties, such as $\mathbf{T}^T = \mathbf{T}^-$ and $\mathbf{T}\mathbf{T}^- = \mathbf{T}^-\mathbf{T} = \mathbf{1}$, where $\mathbf{1}$ denotes the identity matrix and $(\cdot)^-$ represents the conjugate transpose of a complex matrix. Therefore we can expand Eq. (7.29) resulting in

$$\mathbf{T}^T \left[\mathbf{K}_{11\mathrm{u}} + jk\mathbf{K}_{12\mathrm{u}} + k^2\mathbf{K}_{22\mathrm{u}} - \omega^2\mathbf{M}_{\mathrm{u}}\right]\mathbf{T}\mathbf{T}^T\mathbf{U} = \mathbf{0}\,. \tag{7.31}$$

The proposed transformation does, however, not change the system matrices $\mathbf{K}_{11\mathrm{u}}$, $\mathbf{K}_{22\mathrm{u}}$, and $\mathbf{M}_{\mathrm{u}}$ which is due to the fact that in their definition provided in Eqs. (7.15), (7.17) and (7.18) the x_1 related terms do not interact with the x_2, x_3 related terms and consequently the following relations hold

$$\mathbf{T}^T\mathbf{K}_{11\mathrm{u}}\mathbf{T} = \mathbf{K}_{11\mathrm{u}}\,, \tag{7.32}$$

$$\mathbf{T}^T\mathbf{K}_{22\mathrm{u}}\mathbf{T} = \mathbf{K}_{22\mathrm{u}}\,, \tag{7.33}$$

$$\mathbf{T}^T\mathbf{M}_{\mathrm{u}}\mathbf{T} = \mathbf{M}_{\mathrm{u}}\,. \tag{7.34}$$

Considering the coupling stiffness matrix $\mathbf{K}_{12\mathrm{u}}$ the transformation has the desired effect that

$$\mathbf{T}^T\mathbf{K}_{12\mathrm{u}}\mathbf{T} = -j\hat{\mathbf{K}}_{12\mathrm{u}} \tag{7.35}$$

where $\hat{\mathbf{K}}_{12\mathrm{u}}$ is a symmetric matrix if we neglect material damping. In principle, the transformation can be thought of as a multiplication of u_{x_1} by the imaginary unit [4]. The final (real-symmetric) form of the SAFE eigenvalue problem is given as

$$\left[\mathbf{K}_{11\mathrm{u}} + k\hat{\mathbf{K}}_{12\mathrm{u}} + k^2\mathbf{K}_{22\mathrm{u}} - \omega^2\mathbf{M}_{\mathrm{u}}\right]\hat{\mathbf{U}} = \mathbf{0}\,, \tag{7.36}$$

where the new nodal displacement vector is defined as

$$\hat{\mathbf{U}} = \mathbf{T}^T\mathbf{U}\,. \tag{7.37}$$

If we now assign real values to k Eq. (7.36) constitutes a standard eigenvalue problem in $\omega(k)$; due to the fact that k is a real value all wave modes are propagating ones [1]. The number of Lamb wave modes that can be computed depends on the number of degrees of freedom n_{dof} of the system. For each wavenumber k_i we obtain n_{dof} propagating modes for which we also determine the mode shape $\hat{\mathbf{U}}_i$. Moreover, the phase velocity c_{p} can be computed from the real part of the wavenumber and the angular frequency as

$$c_{\mathrm{p}} = \frac{\omega}{\mathfrak{Re}(k)}. \tag{7.38}$$

On the other hand, if we are interested in the full spectrum of propagating and evanescent modes, we have to determine the unknown complex wavenumber $k(\omega)$

for a prescribed circular frequency ω. To this end, Eq. (7.36) is usually rewritten in the following form [4]

$$(\mathbf{A} - k\mathbf{B})\,\mathbf{Q} = \mathbf{0}\,, \tag{7.39}$$

where the matrices $\mathbf{A}$ and $\mathbf{B}$ are defined as

$$\mathbf{A} = \begin{bmatrix} \mathbf{0} & \mathbf{K}_{11\mathrm{u}} - \omega^2\mathbf{M}_{\mathrm{u}} \\ \mathbf{K}_{11\mathrm{u}} - \omega^2\mathbf{M}_{\mathrm{u}} & \hat{\mathbf{K}}_{12\mathrm{u}} \end{bmatrix}, \tag{7.40}$$

$$\mathbf{B} = \begin{bmatrix} \mathbf{K}_{11\mathrm{u}} - \omega^2\mathbf{M}_{\mathrm{u}} & \mathbf{0} \\ \mathbf{0} & \mathbf{K}_{22\mathrm{u}} \end{bmatrix}, \tag{7.41}$$

and the vector $\mathbf{Q}$ is given as

$$\mathbf{Q} = \begin{bmatrix} \hat{\mathbf{U}} \\ k\hat{\mathbf{U}} \end{bmatrix}. \tag{7.42}$$

Consequently, the size of the eigenvalue problem is doubled. The computed complex wavenumbers $k = k_{\mathrm{Re}} + jk_{\mathrm{Im}}$ contain the phase velocity as the real part and their amplitude decay is described by the imaginary part [1]. The solution of Eq. (7.36) provides for each circular frequency ω_i the $2n_{\mathrm{dof}}$ eigenvalues k_i^{m} and eigenvectors $\hat{\mathbf{U}}_i$ (right eigenvector). We have to bear in mind that the formulation in Eq. (7.36) is preferred if only the propagating modes are considered [4].

7.1.4.1 Phase and Group Velocities of Guided Waves

After solving the eigenvalue problems in Eqs. (7.36) or (7.39) we can easily compute the phase velocity c_{p} in terms of the real part of the complex wavenumber and the angular frequency, cf. Eq. (7.38). The group velocity c_{g} can be determined if we compute the derivative of the phase velocity with respect to the wave vector $\mathbf{k}$ defined as

$$\mathbf{k} = k\mathbf{d}\,, \tag{7.43}$$

where $\mathbf{d}$ is the propagation direction vector. The final result to compute the group velocity is [17]

$$c_{\mathrm{g}} = \frac{\partial\omega}{\partial k} = \frac{c_{\mathrm{p}}^2}{c_{\mathrm{p}} - \omega\dfrac{\mathrm{d}c_{\mathrm{p}}}{\mathrm{d}\omega}}. \tag{7.44}$$

In the computation of the group velocity we follow the methodology published in [10, 21]. The procedure starts by evaluating the derivative of Eq. (7.36)

$$\frac{\partial}{\partial k}\left(\left[\mathbf{K}_{11\mathrm{u}} + k\hat{\mathbf{K}}_{12\mathrm{u}} + k^2\mathbf{K}_{22\mathrm{u}} - \omega^2\mathbf{M}_{\mathrm{u}}\right]\hat{\mathbf{U}}\right) = \mathbf{0}\,. \tag{7.45}$$

In the next step, we premultiply Eq. (7.45) with the transpose of the so-called left eigenvector $\hat{\mathbf{U}}_{\mathrm{L}}^T$

$$\hat{\mathbf{U}}_{\mathrm{L}}^T\left[\hat{\mathbf{K}}_{12\mathrm{u}} + 2k\mathbf{K}_{22\mathrm{u}} - 2\omega\frac{\partial\omega}{\partial k}\mathbf{M}_{\mathrm{u}}\right]\hat{\mathbf{U}} = \mathbf{0}\,. \tag{7.46}$$

The group velocity can now be computed as

$$c_{\mathrm{g}} = \frac{\hat{\mathbf{U}}_{\mathrm{L}}^T\left(\hat{\mathbf{K}}_{12\mathrm{u}} + 2k\mathbf{K}_{22\mathrm{u}}\right)\hat{\mathbf{U}}}{2\omega\hat{\mathbf{U}}_{\mathrm{L}}^T\mathbf{M}_{\mathrm{u}}\hat{\mathbf{U}}}\,. \tag{7.47}$$

The left eigenvector is determined by solving the following eigenvalue problem

$$\hat{\mathbf{U}}_{\mathrm{L}}^T\left[\mathbf{K}_{11\mathrm{u}} + k\hat{\mathbf{K}}_{12\mathrm{u}} + k^2\mathbf{K}_{22\mathrm{u}} - \omega^2\mathbf{M}_{\mathrm{u}}\right] = \mathbf{0}\,. \tag{7.48}$$

From the result we can conclude that the left eigenvector $\hat{\mathbf{U}}_{\mathrm{L}}$ is the complex conjugate of the right eigenvector $\hat{\mathbf{U}}$

$$\hat{\mathbf{U}}_{\mathrm{L}} = \hat{\mathbf{U}}^{-}\,. \tag{7.49}$$

7.1.4.2 Verification

In this paragraph we demonstrate the performance of the SAFE method by computing the dispersion diagrams for several plates made of different materials. The first simple benchmark problem constitutes the solution of the eigenvalue problem Eq. (7.36) for an aluminum plate (Young's modulus $E = 70\,\mathrm{GPa}$, Poisson's ratio $\nu = 0.33$, mass density $\rho = 2700\,\mathrm{kg/m^3}$). We deploy ten quadratic (one-dimensional) finite elements to discretize the thickness of the plate. In Fig. 7.3 we notice an excellent agreement with the analytical solution.

The accuracy of the computed results naturally depends on the number of finite elements and the basis functions used. Analogous to the FEM we can always increase the accuracy by a *h*- or *p*-refinement. In this chapter we limit our analysis to quadratic basis function. However, the implementation of higher order polynomial functions introduced in Sect. 6.1 is straightforward.

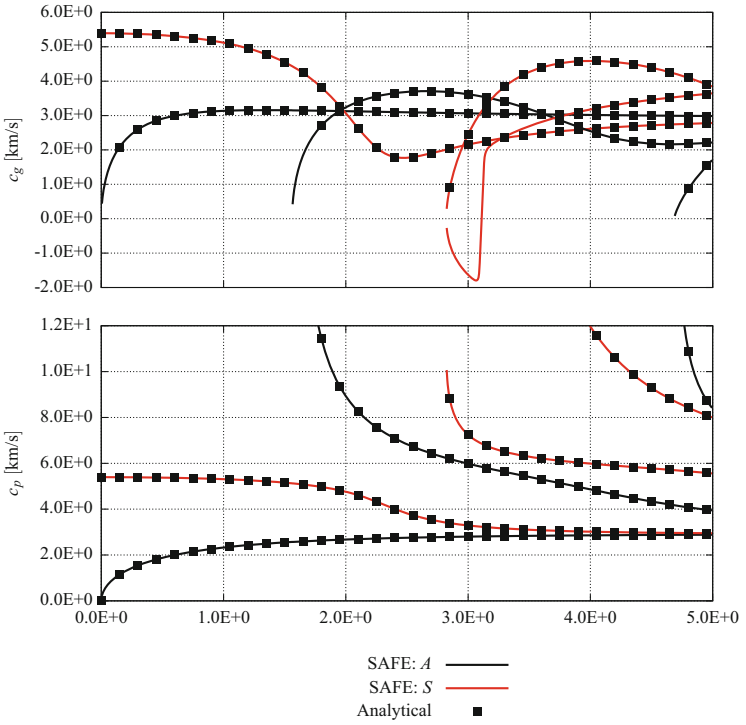

Fig. 7.3 Dispersion curves for an aluminum plate. Comparison between SAFE results and analytical solutions

Figure 7.4 illustrates the effect of a h-extension on the phase velocity. We merely assess the accuracy of the first four Lamb wave modes as this is a typical frequency range that is used in literature for damage detection purposes. The results highlight that three quadratic elements are sufficient to compute highly accurate dispersion curves with a relative error of well below 1% [1]. The number of elements over the thickness of the plate has to be increased if a higher frequency range is of interest.

As a second example we investigate a composite plate made of 16 unidirectional (UD) layers with the following lay up $[0°/45°/90°/-45°]_{s2}$. The plate has an overall thickness of 3.2 mm and the material properties for a UD layer are compiled in Table 7.1. Each ply is discretized with one quadratic finite element. We observe an excellent agreement with the results published in [14], cf. Fig. 7.5. We have to keep in mind that for a CFRP plate the Lamb and the SH wave modes are often coupled.

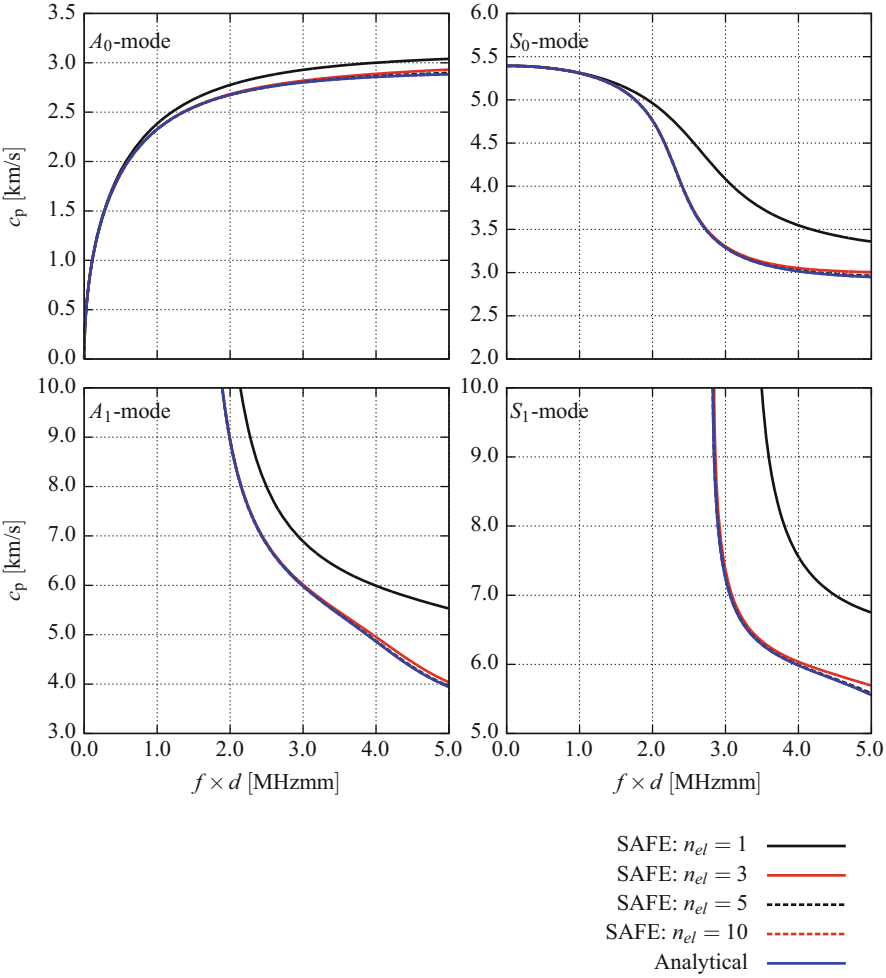

Fig. 7.4 Phase velocity dispersion curves for an aluminum plate for different finite element discretizations

Table 7.1 Material properties of the UD layer at 0° [14]

	E_1	E_2	ν_{12}	ν_{23}	G_{12}	G_{23}	ρ
	in [GPa]	in [GPa]	[–]	[–]	in [GPa]	in [GPa]	in [kg/m^3]
$[UD]_{0°}$	172.0	9.8	0.37	0.55	6.1	3.2	1608

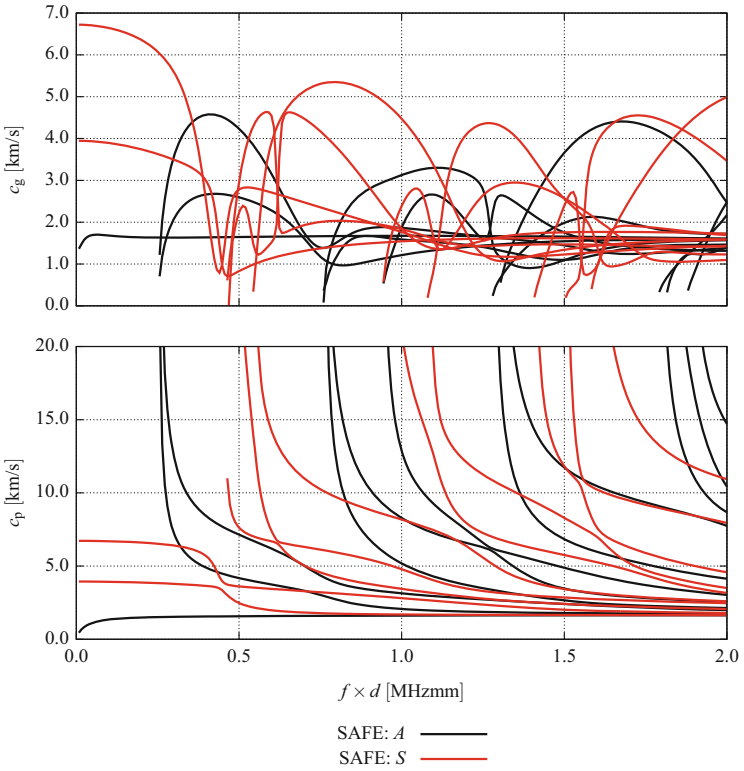

Fig. 7.5 Dispersion curves for a 16-ply CFRP plate

7.1.5 Interaction of Guided Waves with Perturbations

7.1.5.1 General approach

If we want to simulate arbitrary boundary conditions or geometries of plate edges, we have to couple the SAFE method with other numerical approaches. One possibility is to deploy the FEM to account for general perturbations of the plate-like structure [1–3]. The FEM is known for its versatility in modeling geometrically complex systems and therefore we define the boundary conditions, the plate edge, and/or other perturbations in the FE domain as shown in Figs. 7.6 and 7.7, respectively.

The continuity between the SAFE and the FE regions is ensured by using a conformal mesh at the coupling interface(s). In the SAFE method the displacements and the reaction forces at the interface have to be computed. If we now consider an incident wave mode interacting with the edge of a plate, the displacement vector of the reflected wave mode $\mathbf{U}^{\text{reflected}}$ can be approximated by a modal sum of a finite

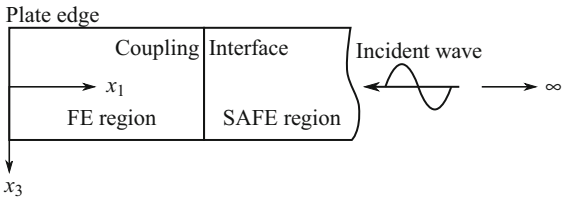

Fig. 7.6 Illustration of the coupling between SAFE and FEM: Reflection of the wave at the edge of the plate

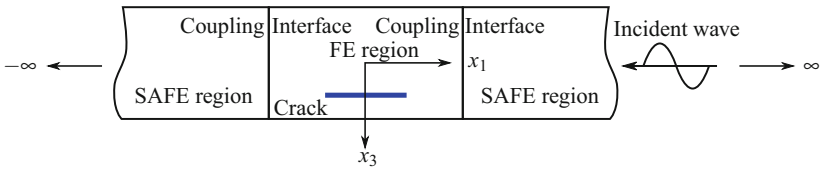

Fig. 7.7 Illustration of the coupling between SAFE and FEM: Interaction of the wave with a crack

number of modes n_r [13]

$$\mathbf{U}^{\text{reflected}} = \sum_{i=1}^{n_\mathrm{r}} b_i \mathbf{U}_i \mathrm{e}^{-jk_i x_1} \ , \tag{7.50}$$

where b_i denotes the amplitude of the ith wave mode and the vector $\mathbf{U}_i$ is the ith eigenvector computed from Eq. (7.14) corresponding to the wavenumber k_i. The approximation of the force is written analogously as

$$\mathbf{F}^{\text{reflected}} = \sum_{i=1}^{n_\mathrm{r}} b_i \boldsymbol{\psi}_i \mathrm{e}^{-jk_i x_1} \ , \tag{7.51}$$

where $\boldsymbol{\psi}_i$ is the force eigenvector which represents the nodal force components due to stresses σ_{x_1} and σ_{x_3} [35]. According to [13] the force eigenvector is given as

$$\boldsymbol{\psi}_i = \left(jk_i \mathbf{K}_{22\mathrm{u}} + \mathbf{K}_{12\mathrm{u}}\right) \mathbf{U}_i \ . \tag{7.52}$$

After having computed the displacement and force vectors due to the reflected wave we still need to determine the following quantities for the incident wave

$$\mathbf{U}^{\text{incident}} = a_i \mathbf{U}_i^{(-)} \ , \tag{7.53}$$

$$\mathbf{F}^{\text{incident}} = a_i \boldsymbol{\psi}_i^{(-)} \ , \tag{7.54}$$

where a_i denotes the amplitude of the ith incident mode. The vectors $\mathbf{U}_i^{(-)}$ and $\boldsymbol{\psi}_i^{(-)}$ are obtained from their corresponding vectors $\mathbf{U}_i$ and $\boldsymbol{\psi}_i$ by negating each component related to the x_1-direction [1]. The overall displacement and force vectors are now computed as

$$\mathbf{U} = \mathbf{U}^{\text{incident}} + \mathbf{U}^{\text{reflected}}, \tag{7.55}$$

$$\mathbf{F} = \mathbf{F}^{\text{incident}} + \mathbf{F}^{\text{reflected}}. \tag{7.56}$$

These quantities can be included in a FEM software to compute the reflection coefficient C_{R}^{ij} for the different propagating wave modes [1, 3, 13]. According to Karunasena et al. [35] we define the reflection coefficient C_{R}^{ij} of the ith reflected mode due to the jth incident mode as

$$C_{\text{R}}^{ij} = \frac{b_i}{a_j}. \tag{7.57}$$

7.1.5.2 Verification

Benchmark examples to demonstrate the applicability of the discussed procedure are studied in the remainder of this section. The finite element stiffness matrix $\mathbf{K}_{\text{u}}^{\text{FE}}$ and mass matrix $\mathbf{M}_{\text{u}}^{\text{FE}}$ are computed by means of the software package Abaqus®. At the boundary between the FE and SAFE regions a conformal discretization is generated. The plate under investigation is made of aluminum (Young's modulus $E = 70\,\text{GPa}$, Poisson's ratio $\nu = 0.33$, mass density $\rho = 2700\,\text{kg/m}^3$) with a thickness of $t = 1\,\text{mm}$. The maximal frequency of interest is 4.5 MHz because in this frequency range only the first four higher order Lamb wave modes exist. In the numerical simulations we only excite the S_0-mode and observe its interaction with the boundary.

Figure 7.8 illustrates the wave reflection behavior at a symmetric plate edge. The term symmetric refers to the midplane of the plate. The infinite plate region is modeled with the help of SAFE, while the edge is discretized using the FEM. From the simulation we determine the edge reflection coefficient $C_{\text{R}} \in [0, 1]$ for the symmetric and antisymmetric modes. Here, one important advantage of the SAFE method can be exploited as each mode can be investigated separately.

As expected only the symmetric mode is reflected and no mode conversion takes place. In Fig. 7.8 we clearly observe the cut-off frequencies of the higher order symmetric Lamb wave modes. Note that the sum of the reflection coefficients of all propagating modes is equal to one.

Figure 7.9 illustrates the wave reflection behavior at an asymmetric plate edge. The plate edge is inclined at an angle of 45°. Because of the asymmetry of the edge geometry mode conversion from the symmetric S_0-mode to the antisymmetric modes A_i is observed. The reflection coefficient illustrates the existence of both symmetric and antisymmetric wave modes after the interaction with the boundary of the plate.

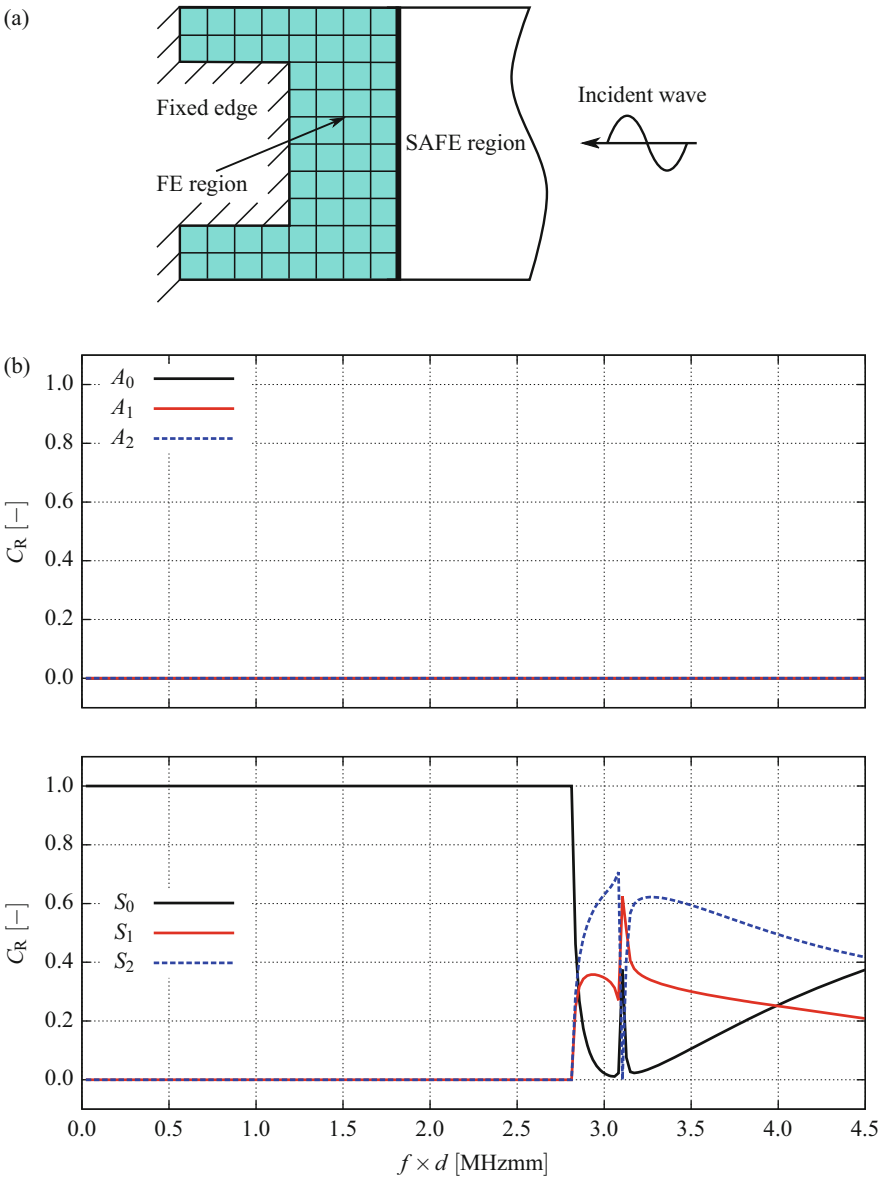

Fig. 7.8 SAFE-FE: Reflection of the S_0-mode at a symmetric plate edge. (**a**) Numerical model. (**b**) Reflection coefficient C_R for the symmetric and antisymmetric guided wave modes

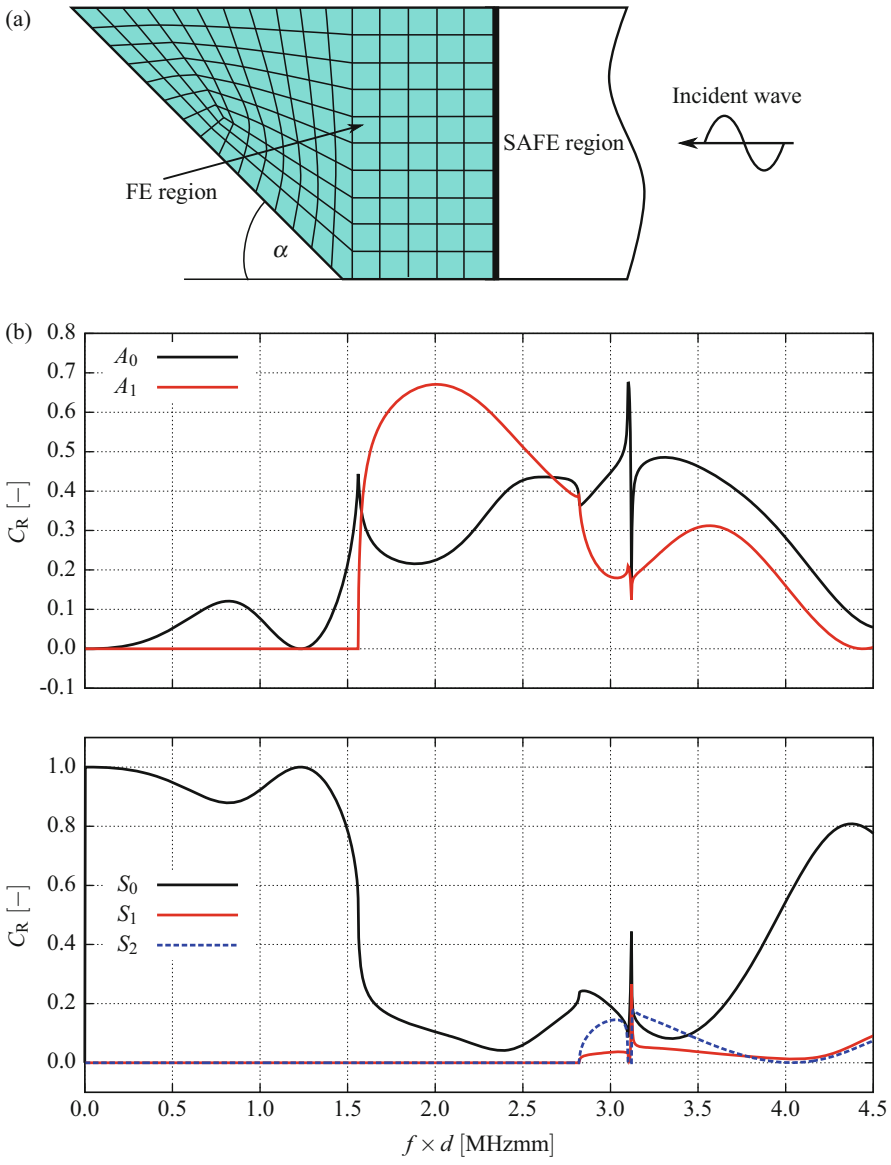

Fig. 7.9 SAFE-FE: Reflection of the S_0-mode at an asymmetric plate edge. (**a**) Numerical model. (**b**) Reflection coefficient C_R for the symmetric and antisymmetric guided wave modes.

7.1.6 Force Response Analysis

7.1.6.1 General approach

In Sects. 7.1.4 and 7.1.5 we have computed the wave motion in an infinite plate and additionally we have included the interaction of the waves with perturbations in the platelike geomerty. This simulations have been executed without applying forces to the structure. In this section we, therefore, focus on the force response analysis. To this end, we include the effect of point forces. This is the most important case as all distributed forces can be decomposed into a set of (energetically equivalent) point forces in the framework of the FEM.

In this section we only discuss the two-dimensional implementation of the force response analysis. To this end, we follow the approach discussed in [9, 42, 44]. We consider the case of an arbitrarily distributed force $\mathbf{f}(t)$ as illustrated in Fig. 7.10. The frequency components of the external force are computed using the Fourier transform

$$\check{\mathbf{f}}(\omega) = \int_{-\infty}^{\infty} \mathbf{f}(t) \mathrm{e}^{-j\omega t} \mathrm{d}t \,. \tag{7.58}$$

The homogeneous equation (7.39) can now be complemented by the force term

$$[\mathbf{A} - k\mathbf{B}(\omega)]\,\mathbf{Q} = \check{\mathbf{F}}(\omega) \,, \tag{7.59}$$

with

$$\check{\mathbf{F}}(\omega) = \begin{bmatrix} \check{\mathbf{f}}(\omega) \\ \mathbf{0} \end{bmatrix} \,. \tag{7.60}$$

The solution of Eq. (7.59) can be expressed in terms of an eigenvector expansion [51]

$$\hat{\mathbf{U}}(k,\omega) = \sum_{i=i}^{4n_{\mathrm{Node}}} \frac{1}{k_i - k}\, \mathbf{Q}_i \, \frac{\mathbf{Q}_i^T \check{\mathbf{F}}}{\mathbf{Q}_i^T \mathbf{B} \mathbf{Q}_i} \,. \tag{7.61}$$

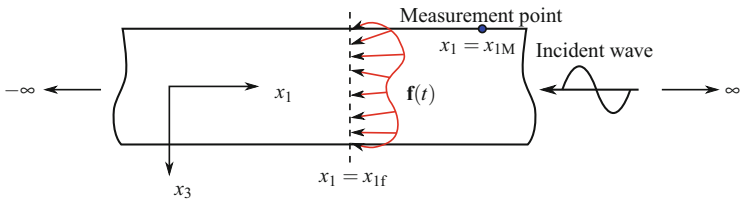

Fig. 7.10 Sketch of the SAFE model for the force response analysis

If n_{Node} is the number of nodes corresponding to the finite element discretization of the cross section of the structure, we can compute $4n_{\text{Node}}$ eigenvalue–eigenvector pairs. To determine the results in the spatio-temporal domain we additionally need to define the spatial as well as the inverse Fourier transforms [9, 42, 44] as

$$\hat{\mathbf{U}}(k,\omega) = \int_{-\infty}^{\infty} \hat{\mathbf{U}}(x,\omega)\mathrm{e}^{jkx_1}\mathrm{d}\,x_1 \ , \tag{7.62}$$

$$\hat{\mathbf{U}}(x,\omega) = \frac{1}{2\pi}\int_{-\infty}^{\infty} \hat{\mathbf{U}}(k,\omega)\mathrm{e}^{-jkx_1}\mathrm{d}k \ . \tag{7.63}$$

Accordingly, we obtain the solution in the x_1-domain by applying the inverse Fourier transform to Eq. (7.61) as

$$\hat{\mathbf{U}}(x_1,\omega) = \frac{1}{2\pi}\sum_{i=i}^{4n_{\text{Node}}}\int_{-\infty}^{\infty}\frac{1}{k_i-k}\,\mathbf{Q}_i\,\frac{\mathbf{Q}_i^T\check{\mathbf{F}}}{\mathbf{Q}_i^T\mathbf{B}\mathbf{Q}_i}\mathrm{e}^{-jk_ix_1}\mathrm{d}k \ . \tag{7.64}$$

Equation (7.64) is now solved with the help of Cauchy's theorem of residues [42]. The solution depends on the location of the measurement point $x_{1\text{M}}$ with respect to the excitation point $x_{1\text{f}}$, cf. Fig. 7.10. We consider the case where $x_{1\text{M}} > x_{1\text{f}}$

$$\hat{\mathbf{U}}(x_1,\omega)|_{x_{1\text{M}}>x_{1\text{f}}} = -j\sum_{i=i}^{2n_{\text{Node}}}\mathbf{Q}_i\,\frac{\mathbf{Q}_i^T\check{\mathbf{F}}}{\mathbf{Q}_i^T\mathbf{B}\mathbf{Q}_i}\mathrm{e}^{-jk_i\check{x}_1} \ , \tag{7.65}$$

with

$$\check{x}_1 = x_{1\text{M}} - x_{1\text{f}} \ . \tag{7.66}$$

Due to the requirement that the displacements should be bounded, we only sum over those modes that have real wavenumbers or complex wavenumbers with a positive imaginary part. The time-domain response is then computed by using the inverse Fourier transform as [1]

$$\hat{\mathbf{U}}(x_1,t) = \frac{1}{2\pi}\int_{-\infty}^{\infty}\hat{\mathbf{U}}(x_1,\omega)\mathrm{e}^{j\omega t}\mathrm{d}\omega \ . \tag{7.67}$$

The extension to three-dimensional systems is discussed in [1, 42]. There, also an alternative approach, based on a convolution integral, is explained. Furthermore, an extension to account for edge reflections is also possible [1].

7.1.6.2 Verification

The excitation of the guided waves is achieved by means of a perfectly bonded thin actuator. Instead of modeling the transducer itself we apply the simplified force model developed in [16, 18]. Therefore, the actuator is modeled as two point forces acting in opposite directions at the end of the actuator edges.

The time response simulations are performed for a 1 mm thick aluminum plate (material properties: Young's modulus $E = 70\,\text{GPa}$, Poisson's ratio $\nu = 0.33$, mass density $\rho = 2700\,\text{kg/m}^3$) with a 6 mm long actuator attached on the top surface, as shown in Fig. 7.11. For the current example we choose an excitation frequency of $f_{\text{ex}} = 250\,\text{kHz}$ for the five cycle sine burst signal given in Eq. (6.37). At this

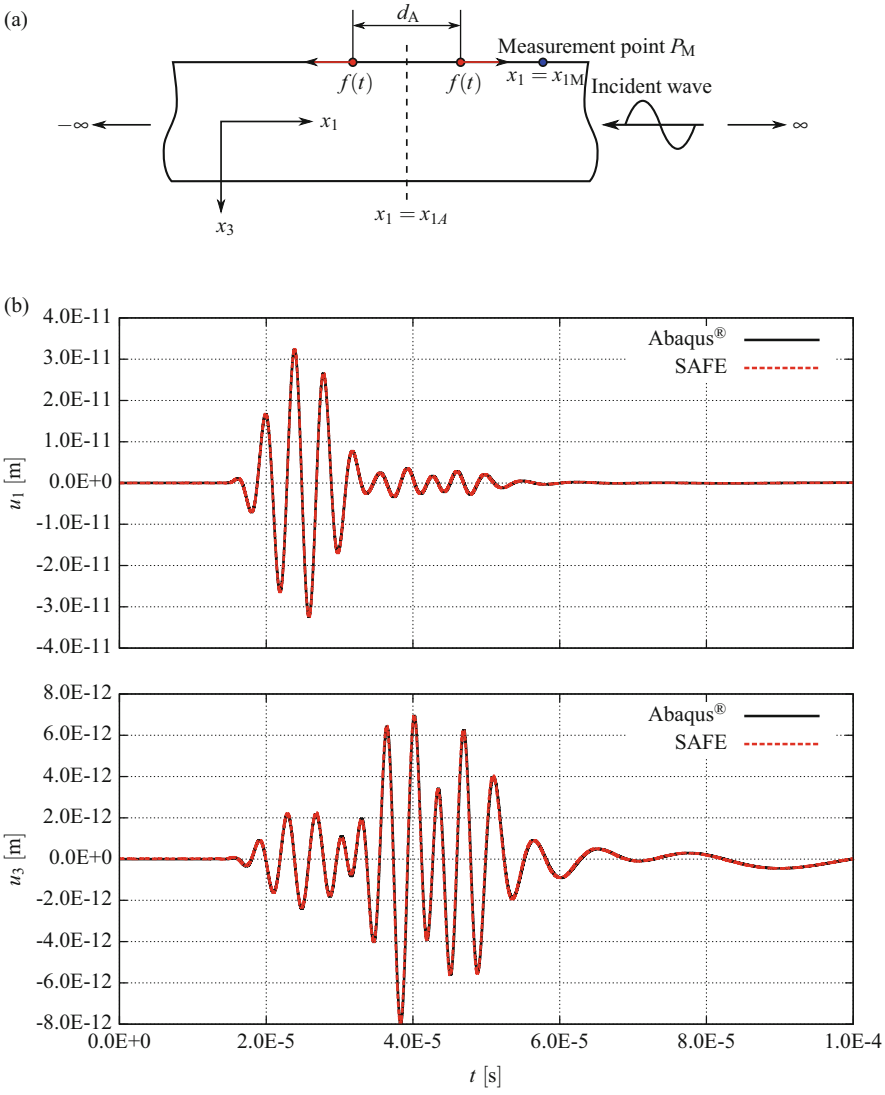

Fig. 7.11 Force response analysis: Two-dimensional model of a perfectly bonded actuator. (**a**) Numerical model. (**b**) In-plane (u_1) and out-of-plane (u_3) displacements at the measurement point P_M

frequency only the two fundamental Lamb wave modes are present in the plate. A comparison of the displacement history at the measurement point P_{M}, which is located at a distance of 80 mm from the excitation source is obtained by using the SAFE method and Abaqus® and shows an excellent agreement.

7.1.7 Summary

The SAFE method combines the versatility of FE-based approaches with the advantages of purely analytical solutions. Using this method the material properties can vary in the thickness direction of the plate, while infinite dimensions are assumed otherwise. To this end, the thickness is discretized using a conventional FE ansatz. Regarding the wave propagation direction we deploy complex-valued exponential functions. For plane waveguides, only one-dimensional (1D) elements are needed. Each material layer in the plate is represented by at least one 1D element. 2D elements, however, are needed for modeling complex, 3D waveguides. The SAFE method is formulated in the frequency domain similar to analytical approaches. The computational effort is significantly reduced compared to the fully three-dimensional FEM due to the fact that the dimensionality of the problem is reduced. However, if we want to recover the displacement field in the time-domain, an inverse Fourier transform has to be evaluated. One main advantage shared by both analytical and semi-analytical methods is that each mode can be considered individually. This allows a detailed analysis of the wave propagation behavior, since specific modes of interest can be considered separately in further stages of the analysis. Generally speaking these types of methods are applicable to [63]:

1. The investigation of the behavior of a single mode.
2. The efficient computation of dispersion diagrams.
3. The computation of the displacement fields if only a small area is of interest.

7.2 Coupling of Analytical Solutions and the Spectral Element Method in the Frequency Domain

The content of this section is primarily based on Dr. Vivar-Perez' research. The results of his investigations are published in a PhD thesis [58] and in two peer-reviewed journal articles [59, 60].

7.2.1 Motivation

The application of purely analytical methods is very convenient when dealing with wave propagation problems in large homogeneous structures. From a computational

point of view, the computation of analytical solutions is rather inexpensive. On the other hand, analytical methods are only suitable for certain geometries and they are derived mostly in the frequency domain. Therefore, many researchers favor the use of purely numerical methods, such as the finite element method (FEM) to deal with more general problems. The main advantage of the FEM lies in its flexibility to model arbitrarily shaped domains and to obtain solutions in the time-domain [58]. However, they are numerically more expensive and involve a higher number of degrees of freedom in comparison to the same computation using analytical methods. Consequently, we promote the development of hybrid methods that only deploy analytical approaches in large areas of the model that are unperturbed and suitable for this purpose. Therefore, only specific details that are of interest to the analyst need to be resolved by numerical approaches.

To attain our goal we seize ideas that were proposed by Karmazin [30, 31] and Glushkov et al. [19, 20]. They have analyzed the wave propagation in a plate in the frequency domain and obtained the solution to the system of partial differential equations in terms of the fundamental solution or Green's tensor. To this end, Cauchy's theorem of residues is applied. We then derive integral expressions which can be used to compute the response of the plate due to an arbitrary distribution of loads. This approach can naturally also be used to describe wave reflections at boundaries and defects. Similar ideas have already been presented in Sect. 7.1 in the context of the SAFE method.

The novelty of our approach lies in the fact that instead of using standard FEM to model the perturbations of the plate [6, 25] we deploy the spectral element method (SEM) which has a higher order of accuracy [5, 12, 56]. Furthermore, we determine the bonding conditions between the numerical model of the perturbation and the analytical model of the plate in the frequency domain by means of an analytical ansatz. With the help of quadrature formulae and the SEM we discretize the set of coupling equations and derive semi-analytical expressions for the propagation of guided waves. To this end, we exploit the concept of the dynamic reaction or response matrix of the plate with exact wavenumbers. The inherent advantage of using exact wavenumbers instead of approximated ones is to be seen in the increased accuracy of the final results. Additionally, no discretization through the thickness of the plate has been used in contrast to the works presented by Loveday [42], Ahmad [1], or Morvan et al. [47].

7.2.2 Definition of the Problem

In the following we derive the coupling equations to account for the bonding of a piezoelectric transducer to an isotropic (infinite) plate. Accordingly, the transducer and the plate share a common surface denoted by Γ_{C}. A schematic representation of the problem under consideration is shown in Fig. 7.12.

The behavior of the piezoelectric transducer and of the plate are analyzed separately. To couple both systems we apply specific boundary conditions on the

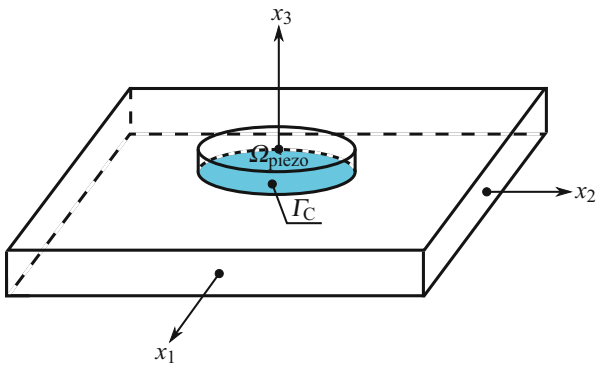

Fig. 7.12 Schematic representation and reference coordinate system of a piezoelectric patch bonded to a plate. The piezoelectric patch occupies a volume Ω_{piezo} and shares a common interface Γ_{C} with the plate

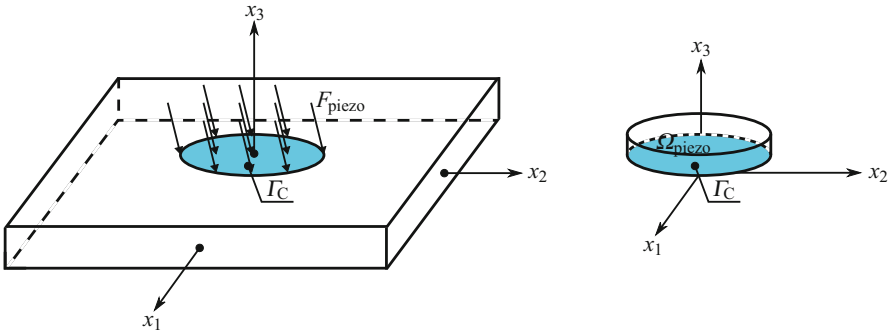

Fig. 7.13 Separate analyses of the dynamic response of the plate and the piezoelectric transducer are executed. The influence of the transducer on the plate is modeled as a transient load $\mathbf{F}_{\text{piezo}}$ acting on Γ_{C}. To account for the coupling of both systems specific boundary conditions are applied at the interface representing the reaction forces of the plate acting on the transducer

common interface Γ_{C}. To this end, we first compute the displacements of the infinite plate due to mechanical loads acting on Γ_{C}. Second, we analyze the mechanical displacements and the electric potential of the piezoelectric transducer due to certain boundary conditions applied on Γ_{C}. These conditions describe the influence of the reaction forces exerted by the plate on the transducer. The basic idea is illustrated in Fig. 7.13.

In Sect. 7.2.3 we discuss how to analytically compute the displacements of an infinite plate due to an arbitrary distribution of loads. To this end, we consider the governing equations and boundary conditions presented in Sect. 4.1 and transform them into the frequency domain. Thereafter, we derive appropriate boundary conditions that need to be applied on the common interface Γ_{C}, see Sect. 7.2.4.

7.2.3 Analytical Solution to the Wave Propagation Problem in Isotropic Plates

For the sake of clarity and completeness, we repeat Navier's equation for a three-dimensional isotropic body

$$(\lambda + \mu)\,\nabla\nabla\cdot\mathbf{u} + \mu\Delta\mathbf{u} = \rho\ddot{\mathbf{u}}\ . \tag{7.68}$$

The coefficients λ and μ denote Lame's constants and ρ is the mass density. The displacement vector $\mathbf{u}$ is a function of the position vector $\mathbf{x}$ and the time t. The differential operators ∇ and Δ represent spatial derivatives according to the Nabla operator and Laplace's operator, while an overdot $\dot{(\cdot)}$ denotes a temporal derivative. In the following we assume that the plate has infinite dimensions in the x_1-x_2-plane and regarding the x_3-direction it is bounded by two parallel surfaces at $x_3 = \pm d/2$. We account for the influence of external loads $\mathbf{F}_{\text{ext}}$ (applied to the upper surface) by introducing Neumann boundary conditions

$$\left[\mu\left(\nabla u_3 + \mathbf{u}_{,3}\right) + \lambda\nabla\cdot\mathbf{u}\mathbf{e}_3\right]_{x_3=+d/2} = \mathbf{F}_{\text{ext}}\ , \tag{7.69}$$

$$\left[\mu\left(\nabla u_3 + \mathbf{u}_{,3}\right) + \lambda\nabla\cdot\mathbf{u}\mathbf{e}_3\right]_{x_3=-d/2} = \mathbf{0}\ , \tag{7.70}$$

where $\mathbf{e}_i$ stands for the unit normal vector in x_i-direction and the notation $(\cdot)_{,i}$ represents the partial derivative with respect to x_i.

7.2.3.1 Analytical Approach

As mentioned before we consider the solution to Navier's equation in the frequency domain. Therefore, we have to apply the Fourier transform to the displacement vector and the load vector

$$\check{\mathbf{u}}(\bar{\mathbf{x}}, x_3, \omega) = \int_{-\infty}^{\infty}\mathbf{u}(\bar{\mathbf{x}}, x_3, t)\mathrm{e}^{j\omega t}\mathrm{d}t\ , \tag{7.71}$$

$$\check{\mathbf{F}}_{\text{ext}}(\bar{\mathbf{x}}, \omega) = \int_{-\infty}^{\infty}\mathbf{F}_{\text{ext}}(\bar{\mathbf{x}}, t)\mathrm{e}^{j\omega t}\mathrm{d}t\ . \tag{7.72}$$

For reasons that will become apparent in the course of this section we divide the position vector into two parts that correspond to the in-plane components $\bar{\mathbf{x}}$ and an out-of-plane component x_3 with respect to the infinite plate

$$\bar{\mathbf{x}} = x_1\mathbf{e}_1 + x_2\mathbf{e}_2\ , \tag{7.73}$$

$$\mathbf{x} = \bar{\mathbf{x}} + x_3\mathbf{e}_3\ . \tag{7.74}$$

Now the governing equations (7.68) and the boundary conditions (7.69) and (7.70) can be expressed in terms of the circular frequency ω

$$(\lambda + \mu)\,\nabla\nabla\cdot\check{\mathbf{u}} + \mu\Delta\check{\mathbf{u}} = -\rho\omega^2\check{\mathbf{u}}\,. \tag{7.75}$$

We have to bear in mind that any temporal derivation is replaced by a multiplication with $j\omega$ when we operate in the frequency domain. Here, $j = \sqrt{-1}$ denotes the imaginary unit. The boundary conditions are basically unchanged and are given as

$$\left[\mu\left(\nabla\check{u}_3 + \check{\mathbf{u}}_{,3}\right) + \lambda\nabla\cdot\check{\mathbf{u}}\mathbf{e}_3\right]_{x_3=+d/2} = \check{\mathbf{F}}_{\text{ext}}\,, \tag{7.76}$$

$$\left[\mu\left(\nabla\check{u}_3 + \check{\mathbf{u}}_{,3}\right) + \lambda\nabla\cdot\check{\mathbf{u}}\mathbf{e}_3\right]_{x_3=-d/2} = \mathbf{0}\,. \tag{7.77}$$

The solution to Eq. (7.75) satisfying the boundary conditions Eqs. (7.76) and (7.77) can be found in terms of the external load $\check{\mathbf{F}}_{\text{ext}}$ using the concept of Green's tensor also known as response tensor

$$\check{\mathbf{u}}(\bar{\mathbf{x}}, x_3, \omega) = \int_{\mathbb{R}^2} \check{\mathbf{E}}(\bar{\mathbf{x}} - \bar{\mathbf{x}}', x_3, \omega)\cdot\check{\mathbf{F}}_{\text{ext}}(\bar{\mathbf{x}}', \omega)\mathrm{d}\bar{\mathbf{x}}'\,, \tag{7.78}$$

where $\bar{\mathbf{x}}'$ is the in-plane position vector of the applied load. Since it is possible to derive a closed-form analytical expression for the frequency-dependent response tensor $\check{\mathbf{E}}$, we can also solve Eq. (7.78) for the displacement vector. A detailed derivation is found in [58] and similar procedures have also been published in [30, 31, 61]. In the remainder of this section we sketch the solution algorithm for the two-dimensional problem.

7.2.3.2 Two-Dimensional Problem

The statement of the problem is simplified by considering a distribution of loads that is only dependent on the spatial variable x_ξ as illustrated in Fig. 7.14. The

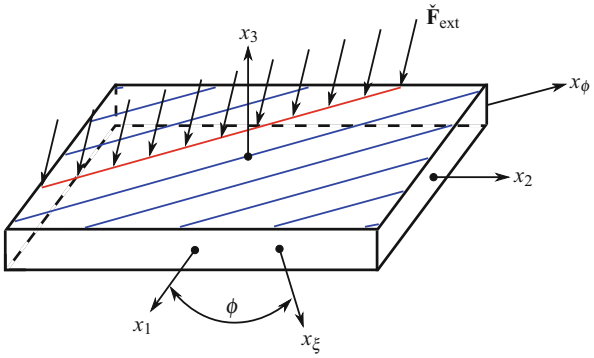

Fig. 7.14 Distribution of a line load and rotation of the coordinate system

rotated coordinate system (x_ξ, x_ϕ, x_3) is obtained by a counterclockwise rotation about the x_3-axis. The rotation angle ϕ depends on the orientation of the distributed load. Therefore, all dependencies on the spatial variable x_ϕ can be neglected and Eq. (7.78) is given as

$$\breve{\mathbf{u}}(\bar{\mathbf{x}}, x_3, \omega) = \int_{\mathbb{R}^2} \breve{\mathbf{E}}(x_\xi - x'_\xi, x_3, \omega) \cdot \breve{\mathbf{F}}_{\text{ext}}(x'_\xi, \omega) \mathrm{d}\, x'_\xi \,. \tag{7.79}$$

According to Vivar-Perez [58] Green's tensor can be determined under these conditions using the following expression

$$\begin{aligned} \breve{\mathbf{E}}(x_\xi, x_3, \omega) = \sum_{n=0}^{\infty} \Big[& \mathbf{E}^{\mathrm{A}}(x_3, k_{\mathrm{n}}^{\mathrm{A}}, \omega) \mathrm{e}^{jk_{\mathrm{n}}^{\mathrm{A}} x_\xi} + \mathbf{E}^{\mathrm{S}}(x_3, k_{\mathrm{n}}^{\mathrm{S}}, \omega) \mathrm{e}^{jk_{\mathrm{n}}^{\mathrm{S}} x_\xi} \\ & + \mathbf{E}^{\mathrm{a}}(x_3, k_{\mathrm{n}}^{\mathrm{a}}, \omega) \mathrm{e}^{jk_{\mathrm{n}}^{\mathrm{a}} x_\xi} + \mathbf{E}^{\mathrm{s}}(x_3, k_{\mathrm{n}}^{\mathrm{s}}, \omega) \mathrm{e}^{jk_{\mathrm{n}}^{\mathrm{s}} x_\xi} \Big] \,, \end{aligned} \tag{7.80}$$

where $\mathbf{E}^{\mathrm{A}}$, $\mathbf{E}^{\mathrm{S}}$, $\mathbf{E}^{\mathrm{a}}$, and $\mathbf{E}^{\mathrm{s}}$ denote the response matrices for the antisymmetric and symmetric Lamb wave (capital letter) and shear horizontal (SH) modes (lower case letter), respectively. These quantities depend on the material properties, the excitation frequency, the geometry of the structure, and the wavenumbers $k_{\mathrm{n}}^{\mathrm{A}}$, $k_{\mathrm{n}}^{\mathrm{S}}$, $k_{\mathrm{n}}^{\mathrm{a}}$ and $k_{\mathrm{n}}^{\mathrm{s}}$. It is important to notice that we are able to pre-compute all these parameters [58]. The two wavenumbers $k_{\mathrm{n}}^{\mathrm{A}}$ and $k_{\mathrm{n}}^{\mathrm{S}}$ are solutions to the Rayleigh-Lamb dispersion equations for the symmetric and antisymmetric modes

$$4k^2 pq \cos\frac{pd}{2}\sin\frac{qd}{2} + [k^2 - q^2]^2 \sin\frac{pd}{2}\cos\frac{qd}{2} = 0 \,, \tag{7.81}$$

$$4k^2 pq \sin\frac{pd}{2}\cos\frac{qd}{2} + [k^2 - q^2]^2 \cos\frac{pd}{2}\sin\frac{qd}{2} = 0 \,. \tag{7.82}$$

The two wavenumbers $k_{\mathrm{n}}^{\mathrm{a}}$ and $k_{\mathrm{n}}^{\mathrm{s}}$, on the other side, are solutions for the shear horizontal modes which can be computed explicitly using

$$k_{\mathrm{n}}^{\mathrm{a}} = \sqrt{\frac{\omega^2}{c_2^2} - \frac{(2n+1)^2\pi^2}{d^2}} \,, \tag{7.83}$$

$$k_{\mathrm{n}}^{\mathrm{s}} = \sqrt{\frac{\omega^2}{c_2^2} - \frac{4n^2\pi^2}{d^2}} \,, \tag{7.84}$$

where p, q, c_1, and c_2 are defined as

$$p = \sqrt{\frac{\omega^2}{c_1^2} - k^2}\,, \tag{7.85}$$

$$q = \sqrt{\frac{\omega^2}{c_2^2} - k^2}\,, \tag{7.86}$$

$$c_1 = \sqrt{\frac{\lambda + \mu}{\rho}}\,, \tag{7.87}$$

$$c_2 = \sqrt{\frac{\mu}{\rho}}\,. \tag{7.88}$$

Equations (7.81) and (7.82) are implicit functions of the wavenumber and the circular frequency. These equations are numerically solved by means of tracking the individual wavenumber branches for each wave mode and each positive value of the frequency. The algorithm is based on a combination of Muller's method [49], used to find the complex roots of Eqs. (7.81) and (7.82) and a procedure to trace implicit planar curves [65]. In the next step, we compute the response matrices $\mathbf{E}^{\mathrm{A}}$, $\mathbf{E}^{\mathrm{S}}$, $\mathbf{E}^{\mathrm{a}}$, and $\mathbf{E}^{\mathrm{s}}$ for each single mode. In the two-dimensional case shown here the matrix functions are given as

$$\mathbf{E}^{\mathrm{A}}(x_3, k_{\mathrm{n}}^{\mathrm{A}}, \omega) = \frac{j}{2\mu \dfrac{\partial D_{\mathrm{A}}}{\partial k}} \begin{bmatrix} N_{\mathrm{kk}}^{\mathrm{A}} & 0 & N_{\mathrm{k3}}^{\mathrm{A}} \\ 0 & 0 & 0 \\ N_{\mathrm{3k}}^{\mathrm{A}} & 0 & N_{\mathrm{33}}^{\mathrm{A}} \end{bmatrix} \Bigg|_{k=k_{\mathrm{n}}^{\mathrm{A}}}\,, \tag{7.89}$$

$$\mathbf{E}^{\mathrm{S}}(x_3, k_{\mathrm{n}}^{\mathrm{S}}, \omega) = \frac{j}{2\mu \dfrac{\partial D_{\mathrm{S}}}{\partial k}} \begin{bmatrix} N_{\mathrm{kk}}^{\mathrm{S}} & 0 & N_{\mathrm{k3}}^{\mathrm{S}} \\ 0 & 0 & 0 \\ N_{\mathrm{3k}}^{\mathrm{S}} & 0 & N_{\mathrm{33}}^{\mathrm{S}} \end{bmatrix} \Bigg|_{k=k_{\mathrm{n}}^{\mathrm{S}}}\,, \tag{7.90}$$

$$\mathbf{E}^{\mathrm{a}}(x_3, k_{\mathrm{n}}^{\mathrm{a}}, \omega) = \frac{j(-1)^n}{\mu k_{\mathrm{n}}^{\mathrm{a}} d} \sin\frac{(2n+1)\pi x_3}{d} \begin{bmatrix} 0 & 0 & 0 \\ 0 & 1 & 0 \\ 0 & 0 & 0 \end{bmatrix}\,, \tag{7.91}$$

$$\mathbf{E}^{\mathrm{s}}(x_3, k_{\mathrm{n}}^{\mathrm{s}}, \omega) = \frac{j(-1)^n}{\kappa_{\mathrm{n}} \mu k_{\mathrm{n}}^{\mathrm{s}} d} \cos\frac{2n\pi x_3}{d} \begin{bmatrix} 0 & 0 & 0 \\ 0 & 1 & 0 \\ 0 & 0 & 0 \end{bmatrix}\,, \tag{7.92}$$

where $\kappa_0 = 2$ and $\kappa_n = 1$ for $n \geq 1$. In the definitions of the response matrices $\mathbf{E}^{\mathrm{A}}$ and $\mathbf{E}^{\mathrm{S}}$ we introduced a set of functions N which is given as

$$N_{\mathrm{kk}}^{\mathrm{A}}(x_3,k,\omega) = q\left[2k^2 \sin\frac{qd}{2}\sin px_3 - (k^2-q^2)\sin\frac{pd}{2}\sin qx_3\right], \tag{7.93}$$

$$N_{\mathrm{kk}}^{\mathrm{S}}(x_3,k,\omega) = q\left[-2k^2 \cos\frac{qd}{2}\cos px_3 + (k^2-q^2)\cos\frac{pd}{2}\cos qx_3\right], \tag{7.94}$$

$$N_{\mathrm{3k}}^{\mathrm{A}}(x_3,k,\omega) = -jk\left[2pq \sin\frac{qd}{2}\cos px_3 + (k^2-q^2)\sin\frac{pd}{2}\cos qx_3\right], \tag{7.95}$$

$$N_{\mathrm{3k}}^{\mathrm{S}}(x_3,k,\omega) = -jk\left[2pq \cos\frac{qd}{2}\sin px_3 + (k^2-q^2)\cos\frac{pd}{2}\sin qx_3\right], \tag{7.96}$$

$$N_{\mathrm{k3}}^{\mathrm{A}}(x_3,k,\omega) = jk\left[(k^2-q^2)\cos\frac{qd}{2}\sin px_3 + 2pq\cos\frac{pd}{2}\sin qx_3\right], \tag{7.97}$$

$$N_{\mathrm{k3}}^{\mathrm{S}}(x_3,k,\omega) = jk\left[(k^2-q^2)\sin\frac{qd}{2}\cos px_3 + 2pq\sin\frac{pd}{2}\cos qx_3\right], \tag{7.98}$$

$$N_{\mathrm{33}}^{\mathrm{A}}(x_3,k,\omega) = p\left[(k^2-q^2)\cos\frac{qd}{2}\cos px_3 - 2k^2\cos\frac{pd}{2}\cos qx_3\right], \tag{7.99}$$

$$N_{\mathrm{33}}^{\mathrm{S}}(x_3,k,\omega) = p\left[-(k^2-q^2)\sin\frac{qd}{2}\cos px_3 + 2k^2\sin\frac{pd}{2}\cos qx_3\right]. \tag{7.100}$$

Additionally, we need to define the functions D

$$D_{\mathrm{A}} = 4k^2pq\cos\frac{pd}{2}\sin\frac{qd}{2} + [k^2-q^2]^2\sin\frac{pd}{2}\cos\frac{qd}{2}, \tag{7.101}$$

$$D_{\mathrm{S}} = 4k^2pq\sin\frac{pd}{2}\cos\frac{qd}{2} + [k^2-q^2]^2\cos\frac{pd}{2}\sin\frac{qd}{2}. \tag{7.102}$$

Thus, each mode has its corresponding excitation matrix. This formulation is convenient for applications, where only the contribution of one single mode is needed [62].

In principle, the different wavenumbers can assume real or complex values. In case of complex wavenumbers the corresponding modes are evanescent meaning that their amplitude decays with the covered distance. On the other hand, real wavenumbers correspond to propagating modes. It can be shown that for each frequency there is a finite number of propagating modes and the rest are evanescent. In many applications we can neglect the evanescent modes as their contribution to the response matrix given in Eq. (7.80) is insignificant. Therefore, we can truncate the sum depending on a pre-defined error threshold [58]. Another point worth

mentioning is that in isotropic plates the response matrix $\check{\mathbf{E}}$ is independent of the wave propagation direction. Therefore, we assume that $\mathbf{e}_\xi = \mathbf{e}_1$ without loss of generality. In anisotropic plates this is unfortunately not the case. The dispersion curves for an aluminum plate are exemplarily shown in Fig. 7.15.

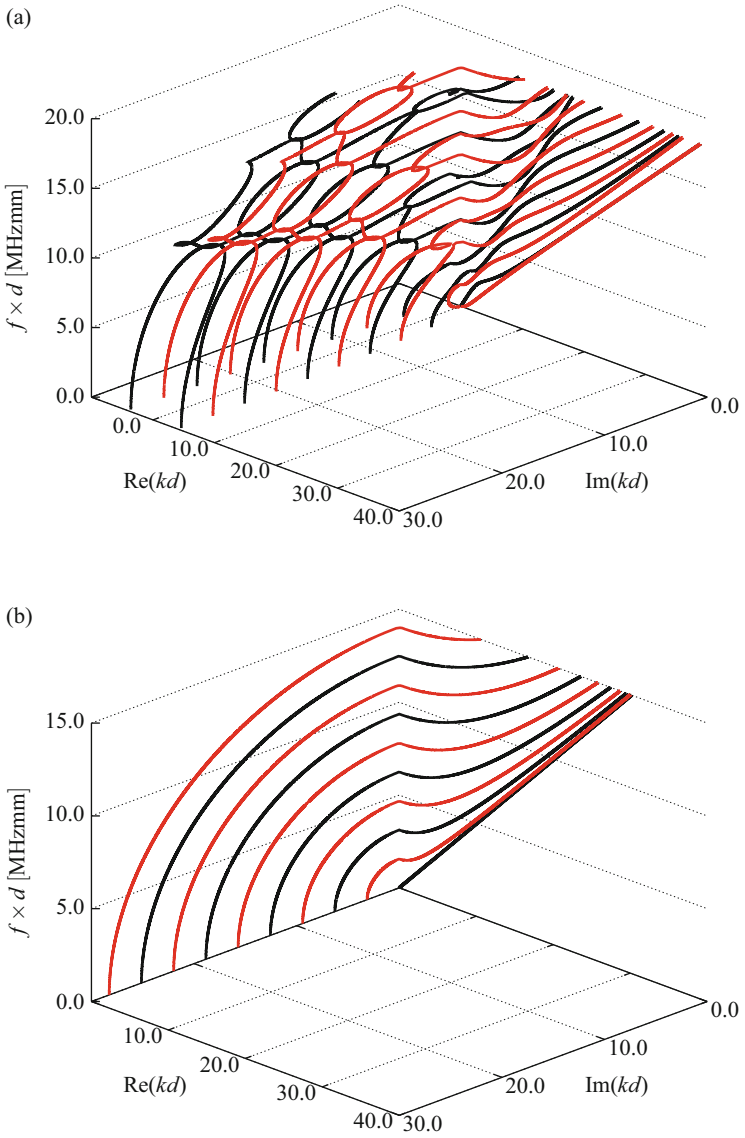

Fig. 7.15 Complex dispersion curves of the Lamb wave and SH modes for an aluminum plate (Young's modulus $E = 70\,\text{GPa}$, Poisson's ratio $\nu = 0.33$, mass density $\rho = 2700\,\text{kg/m}^3$). Symmetric modes are denoted by *black solid lines*, while antisymmetric modes are marked with *red solid lines*. (**a**) Lamb wave modes. (**b**) SH wave modes

7.2.4 Coupling Boundary Conditions

After having studied the analytical solution of an infinite plate under external loading we conduct a separate analysis of the bonded piezoelectric transducer. As already discussed in Chap. 4 piezoelectric materials exhibit a coupling of electrical and mechanical quantities [52, 64]. The mechanical state is characterized by the vector of displacements $\mathbf{u}$, the strain tensor $\boldsymbol{\varepsilon}_\mathrm{u}$, and the stress tensor $\boldsymbol{\sigma}_\mathrm{u}$. On the other hand, the electrical state in a piezoelectric material is given by the electrical potential φ which is a scalar quantity, the electric field vector $\mathbf{E}$, and the vector of electrical displacements $\mathbf{D}$. The governing equations and the constitutive equations for such a material have been presented in Sects. 4.1 and 4.2, respectively.

In order to implement suitable boundary conditions on the interface Γ_C between the infinite plate and the piezoelectric transducer we consider the problem in the frequency domain. We now apply the Fourier transform presented in Eqs. (7.71) and (7.72) to the governing equations (cf. Eqs. (4.1) and (4.2)) and take the constitutive equations (cf. Eqs. (4.14) and (4.15)) of the linear theory of piezoelectricity into account. Therefore, the formulation of the problem in the frequency domain is given in index notation as

$$c_{\mathrm{ijkl}}\check{u}_{\mathrm{k,lj}} + e_{\mathrm{lij}}\check{\varphi}_{\mathrm{,lj}} = -\omega^2\rho\check{u}_i \tag{7.103}$$

$$e_{jkl}\check{u}_{\mathrm{k,lj}} - \kappa_{\mathrm{lj}}\check{\varphi}_{\mathrm{,lj}} = 0. \tag{7.104}$$

Einstein's summation convention regarding the sum over repeated indices k, l, and j is considered and an index j after a comma denotes a partial derivative with respect to the variable x_j. Dirichlet and Neumann boundary conditions are prescribed in the usual way [58, 60].

The interaction between the plate and the transducer is now considered separately. We assume an ideal bonding and therefore both the displacements and the tractions are continuous. The forces in the interface exerted by the piezoelectric transducer on the plate/substrate and the reaction forces of the plate/substrate exerted on the transducer are denoted by $\check{\mathbf{F}}_\mathrm{piezo}$ and therefore we obtain the bonding boundary condition as

$$\left(c_{\mathrm{ijkl}}\check{u}_{\mathrm{k,l}} + e_{\mathrm{lij}}\check{\varphi}_{\mathrm{,l}}\right) n_j|_{\Gamma_\mathrm{C}} + \check{F}_{\mathrm{i,piezo}} = 0\,. \tag{7.105}$$

The displacements of the piezoelectric transducer and the infinite plate are identical on Γ_C. Hence, we can use Eq. (7.78) to obtain an expression to compute the displacements

$$\check{\mathbf{u}}(\bar{\mathbf{x}}, d/2, \omega) = \int_{\mathbb{R}^2} \check{\mathbf{E}}(\bar{\mathbf{x}} - \bar{\mathbf{x}}', d/2, \omega) \cdot \check{\mathbf{F}}_\mathrm{ext}(\bar{\mathbf{x}}', \omega)\mathrm{d}\bar{\mathbf{x}}'\,, \quad \bar{\mathbf{x}}' \in \Gamma_\mathrm{C}. \tag{7.106}$$

Equations (7.105) and (7.106) constrain the plate to account for the dynamical behavior of the piezoelectric transducer and vice versa. Once the system of governing equations restricted to these boundary conditions is solved, we obtain

a solution for the behavior of an isolated piezoelectric patch when it is perfectly bonded to an infinite plate without the need to analyze the behavior of any other point in the plate except for those contained in Γ_C.

The system of partial differential equations given by Eqs. (7.103) and (7.104) can be solved using a FE-based approach, see Chaps. 4 and 6. However, in [58, 60] a collocation approach has been deployed instead of a Bubnov-Galerkin method. In the following we only sketch the basic idea for the case of a transducer which is not bonded to the plate $\check{\mathbf{F}}_{\text{piezo}} = \mathbf{0}$, cf. Eq. (7.105). Therefore, we can set up a linear system of equations in $\check{\mathbf{u}}$ for each frequency

$$\left(\mathbf{K} - \omega^2 \mathbf{M}\right) \check{\mathbf{u}} = \check{\mathbf{F}} \,, \tag{7.107}$$

where $\mathbf{K}$ and $\mathbf{M}$ denote the finite element stiffness and mass matrices, respectively. In the case where the piezoelectric transducer is perfectly bonded to the infinite plate we have to take the reaction forces $\check{\mathbf{F}}_{\text{piezo}}$ into account and their relation to the displacements $\check{\mathbf{u}}$ (cf. Eq. (7.106)). A detailed discussion of the numerical procedure to solve the resulting linear system of equations is provided in [58].

7.2.5 Numerical Results

To demonstrate the properties of the proposed method we consider a two-dimensional problem. A piezoelectric transducer made of PIC-181 (the material data is compiled in Table 7.2) is perfectly bonded to an infinite aluminum plate. The thickness of the transducer is set to $t_p = 1\,\text{mm}$ with a length of $l_p = 10\,\text{mm}$ and the thickness of the aluminum plate is $d = 2\,\text{mm}$, cf. Fig. 7.16. The surfaces of the plate are traction free, and the upper and the lower surface of the piezoelectric

Table 7.2 Material properties for PIC-181

Mechanical properties		Electrical properties	
$C_{11} = C_{22}$	152.3 GPa	e_{31}	−4.5 N/Vm
C_{12}	89.09 GPa	e_{33}	14.9 N/Vm
$C_{13} = C_{23}$	85.42 GPa	e_{15}	11.0 N/Vm
C_{33}	134.1 GPa	κ_{11}^T/κ_0	1224
C_{44}	31.61 GPa	κ_{33}^T/κ_0	1135
$C_{55} = C_{66}$	28.30 GPa		
ρ	7850 kg/m^3		

The poling direction of the material is the x_3-direction. The vacuum permittivity (permittivity of free space) is given by $\kappa_0 = 8.8542 \cdot 10^{-12}$ As/Vm. The values of the non-zero components of the elasticity matrix C_{ij}, the piezoelectric coupling tensor e_{ij}, the dielectric tensor κ_{ij}, and the mass density ρ are given

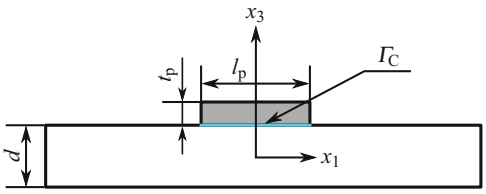

Fig. 7.16 Two-dimensional model of the aluminum plate with a perfectly bonded piezoelectric transducer

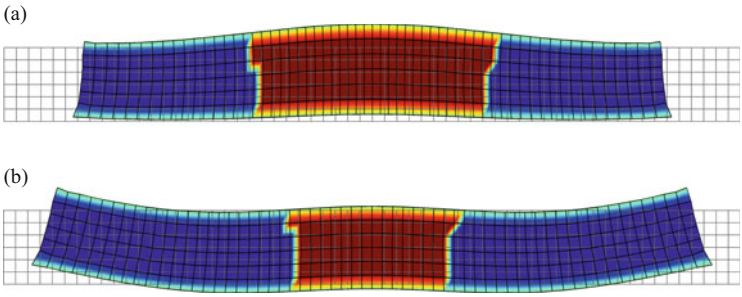

Fig. 7.17 Deformation of the perfectly bonded piezoelectric transducer depicted in Fig. 7.16. The coloring of the contour plots indicates the normalized distribution of the electric potential ϕ. (**a**) $t_1 = 5\,\text{ms}$. (**b**) $t_2 = 10\,\text{ms}$

actuator are electroded. On the lower face of the actuator the potential is fixed ($\phi_l = 0$), while a time dependent voltage signal (cf. Eq. (6.37)) is applied at the upper surface. The center frequency is $f_{ex} = 200\,\text{kHz}$ and three cycles are excited with an amplitude of 50 V.

The piezoelectric transducer is discretized using one spectral element with 567 degrees of freedom ($p_{x_1} = 20$, $p_{x_3} = 8$). To obtain the solution we only considered the first 16 terms in the infinite sum of Eq. (7.80). The simulation results are depicted in Figs. 7.17, 7.18 and 7.19.

With the proposed method, the behavior of the bonded piezoelectric actuator can be analyzed by only considering points located on its domain. Nevertheless the effects of the reaction forces, caused by the elastic plate, on the behavior of the piezoelectric patch are observed. The impact on the bahavior of the plate in the simplified model of the bonded patch is introduced in terms of the response matrix and therefore, the application of our approach is limited to cases where the response matrix can be determined.

To verify the results we compute the displacements at two predefined observation points. Both points are located at the top surface of the plate at $x_1^1 = 200\,\text{mm}$ and at $x_1^2 = 245\,\text{mm}$. We compare the obtained results with finite element computations. To this end, we set up a finite element model in Abaqus® using 8-

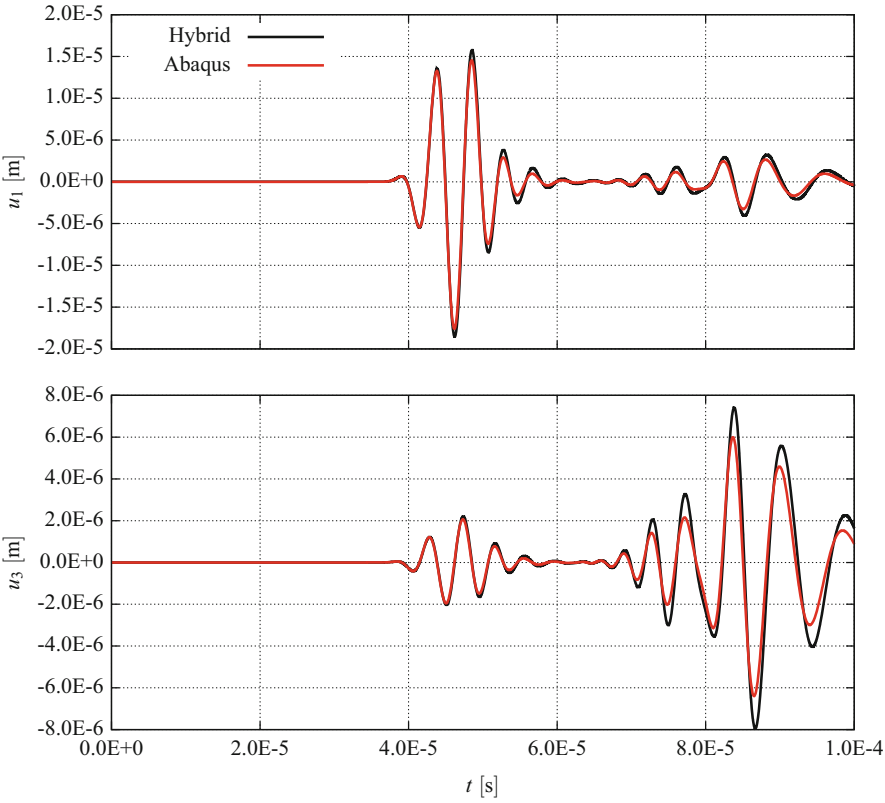

Fig. 7.18 Horizontal and vertical displacement at the first observation point ($x_1 = 200\,\text{mm}$, $x_3 = 1\,\text{mm}$)

noded quadrilateral elements (plane strain conditions are assumed). The element size is $h_{\text{Abaqus}} = 2.510^{-5}\,\text{m}$. We observe that the curves are in good agreement.

This shows the capability of the method to describe the piezoelectric behavior of a sensor/actuator network bonded to a plate. Here, only points lying within the bonding surfaces are considered, i.e. we do not need to discretize the plate itself and we only include points in the interface in the computation. This is very advantageous regarding the simulations of Lamb waves excited by piezoelectric transducers with applications to non-destructive testing. The number of degrees of freedom of the system and the calculation effort are significantly reduced and additionally the analysis of the behavior of the sensor due to the effect of the signals emitted by the actuators is simplified.

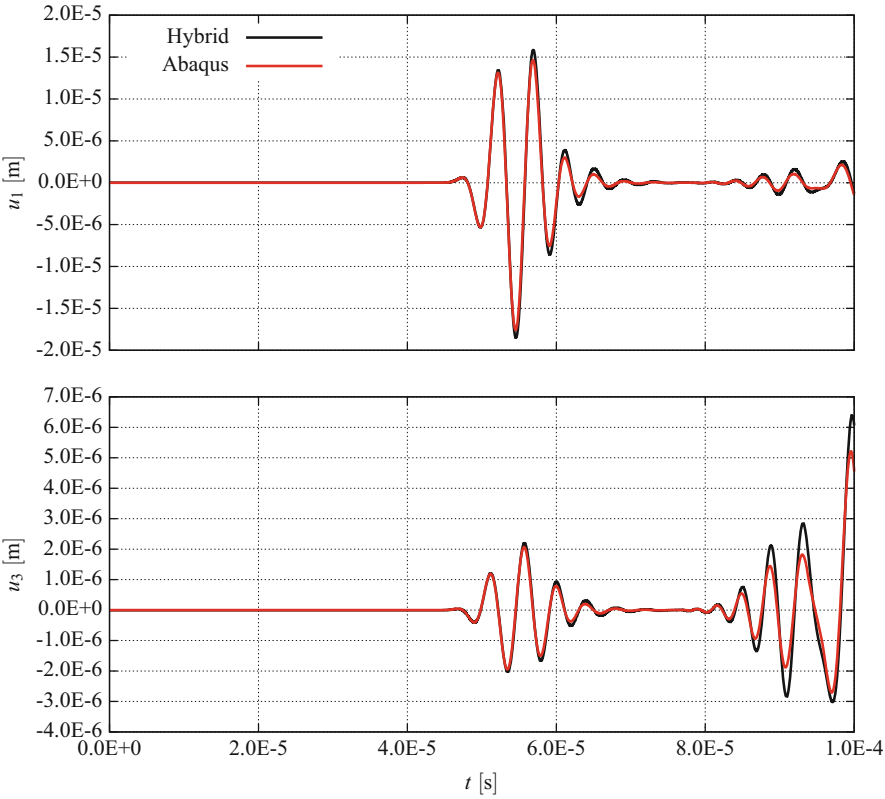

Fig. 7.19 Horizontal and vertical displacement at the second observation point ($x_1 = 245\,\text{mm}$, $x_3 = 1\,\text{mm}$)

References

1. Ahmad ZAB (2011) Numerical simulation of Lamb waves in plates using a semi-analytical finite element method. VDI Fortschritt-Berichte Reihe 20 Nr. 437
2. Ahmad ZAB, Gabbert U (2012) Simulation of Lamb wave reflections at plate edges using the semi-analytical finite element method. Ultrasonics 52:815–820
3. Ahmad ZAB, Vivar Perez JM, Gabbert U (2013) Semi-analytical finite element method for modeling of Lamb wave propagation. CEAS Aeronaut J 4:21–33
4. Bartoli I, Marzani A, di Scalea F, Viola E (2006) Modeling wave propagation in damped waveguides of arbitrary cross-section. J Sound Vib 295:685–707
5. Boyd JP (2000) Chebyshev and Fourier Spectral Methods, 2nd edn. Dover, Mineola
6. Chang Z, Mal A (1999) Scattering of Lamb waves from a rivet hole with edge cracks. Mech Mater 31(3):197–204
7. Chapuis B, Terrien N, Royer D (2010) Excitation and focusing of Lamb waves in a multilayered anisotropic plate. J Acoust Soc Am 127(1):198–203
8. Chitnis M, Desai Y, Shah A, Kant T (2003) Comparisons of displacement-based theories for waves and vibrations in laminated and sandwich composite plates. J Sound Vib 263:617–642

9. Damljanovic V, Weaver R (2004) Forced response of a cylindrical waveguide with simulation of the wavenumber extraction problem. J Acoust Soc Am 115(4):1582–1591
10. Finnveden S (2004) Evaluation of modal density and group velocity by a finite element method. J Sound Vib 273:51–75
11. Fish J, Belytschko T (2007) A first course in finite elements. Wiley, Hoboken
12. Fornberg B (1998) A practical guide to pseudospectral methods. Cambridge monograph on applied and computational mathematics, Cambridge University Press, Cambridge
13. Galan J, Abascal R (2002) Numerical simulation of Lamb wave scattering in semi-infinite plates. Int J Numer Methods Eng 53:1145–1173
14. Gao H (2007) Ultrasonic guided wave mechanics for composite material structural health monitoring. PhD thesis, The Pennsylvania State University
15. Gavric L (1995) Computation of propagative waves in free rail using a finite element technique. J Sound Vib 185(3):531–543
16. Giurgiutiu V (2002) Lamb wave generation with piezoelectric wafer active sensors for structural health monitoring. In: SPIE's 10th Annual International Symposium on Smart Structures and Materials and 8th Annual International Symposium on NDE for Health Monitoring and Diagnostics
17. Giurgiutiu V (2008) Structural health monitoring with piezoelectric active wafer sensors: fundamentals and applications. Elsevier, Amsterdam
18. Giurgiutiu V (2008) Structural health monitoring with piezoelectric wafer active sensors. Academic, Elsevier, Amsterdam
19. Glushkov EV, Glushkova NV, Seemann W, Kvasha OV (2006) Elastic wave excitation in a layer by piezoceramic patch actuators. Acoust Phys 52(4):398–407
20. Glushkov Y, Glushkova N, Krivonos A (2010) The excitation and propagation of elastic waves in multilayered anisotropic composites. J Appl Math Mech 74(3):297–305
21. Han X, Liu GR, Xi ZC, Lam KY (2002) Characteristics of waves in a functionally graded cylinder. Int J Numer Methods Eng 53:653–676
22. Hayashi T (2002) Guided wave animation using semi-analytical finite element method. NDT, pp 75–79
23. Hayashi T, Endoh S (2000) Calculation and visualization of Lamb wave motion. Ultrasonics 38:770–773
24. Hayashi T, Inoue D (2014) Calculation of leaky Lamb waves with a semi-analytical finite element method. Ultrasonics 54:1460–1469
25. Hayashi T, Kawashima K (2002) Multiple reflections of Lamb waves at a delamination. Ultrasonics 40:193–197
26. Hayashi T, Kawashima K, Sun Z, Rose JL (2003) Analysis of flexural mode focusing by a semianalytical finite element method. J Acoust Soc Am 113(3):1241–1248
27. Hayashi T, Song W, Rose J (2003) Guided wave dispersion curves for a bar with an arbitrary cross-section, a rod and rail example. Ultrasonics 41:175–183
28. Hughes TJR (1987) The finite element method: linear static and dynamic finite element analysis. Prentice-Hall, Upper Saddle River
29. Inoue D, Hayashi T (2015) Transient analysis of leaky Lamb waves with a semi-analytical finite element method. Ultrasonics 62:80–88
30. Karmazin A, Kirillova E, Seemann W, Syromyatnikov P (2010) Modelling of 3d steady-state oscillations of anisotropic multilayered structures applying the Green's functions. Adv Theor Appl Mech 3(9):425–445
31. Karmazin A, Kirillova E, Seemann W, Syromyatnikov P (2011) Investigation of Lamb elastic waves in anisotropic multilayered composites applying the Green's matrix. Ultrasonics 51(1):17–28
32. Karunasena W (2004) Numerical modeling of obliquely incident guided wave scattering by a crack in a laminated composite plate. In: Atrens A, Boland J, Clegg R, Griffiths J (eds) Structural integrity and fracture international conference (SIF04), pp 181–187
33. Karunasena W (2008) Elastodynamic reciprocity relations for wave scattering by flaws in fiber-reinforced composite plates. J Mech Mater Struct 3(10):1831–1846

34. Karunasena W, Shah A, Datta S (1991) Wave propagation in a multilayered laminated cross-ply composite plate. Trans. ASME 58:1028–1032
35. Karunasena W, Liew K, Kitipornchai S (1995) Hybrid analysis of Lamb wave reflection by a crack at the fixed edge of a composite plate. Comput Methods Appl Mech Eng 125:221–233
36. Karunasena W, Liew KM, Kitipornchai S (1995) Reflection of plate waves at the fixed edge of a composite plate. J Acoust Soc Am 98(1):644–651
37. Lagasse P (1973) Higher-order finite-element analysis of topographic guides supporting elastic surface waves. J Acoust Soc Am 53(4):1116–1122
38. Li W, Dwight RA, Zhang T (2015) On the study of vibration of a supported railway rail using the semi-analytical finite element method. J Sound Vib 345:121–145
39. Liu GR (2002) A combined finite element/strip element method for analyzing elastic wave scattering by cracks and inclusions in laminates. Comput Mech 28:76–81
40. Liu G, Xi Z (2002) Elastic waves in anisotropic laminates. CRC Press, Boca Raton
41. Loveday P (2006) Numerical comparison of patch and sandwich piezoelectric transducers for transmitting ultrasonic waves. Proc SPIE 6166:616,612
42. Loveday P (2007) Analysis of piezoelectric ultrasonic transducers attached to waveguides using waveguide finite elements. IEEE Trans Ultrason Ferroelectr Freq Control 54(10): 2045–2051
43. Loveday PW (2009) Semi-analytical finite element analysis of elastic waveguides subjected to axial loads. Ultrasonics 49:298–300
44. Loveday P, Long C (2007) Time domain simulation of piezoelectric excitation of guided waves in rails using waveguide finite elements. Proc SPIE 6529:65,290V–1
45. Matt HM (2006) Structural diagnostics of CFRP composite aircraft components by ultrasonic guided waves and built-in piezoelectric transducers. PhD thesis, University of California San Diego
46. Mazzotti M, Bartoli I, Marzani A, Viola E (2013) A coupled SAFE-2.5D BEM approach for the dispersion analysis of damped leaky guided waves in embedded waveguides for arbitrary cross-section. Ultrasonics 53:1227–1241
47. Morvan B, Wilkie-Chancellier N, Duflo H, Trinel A, Duclos J (2003) Lamb wave reflection at the free edge of a plate. J Acoust Soc Am 113(3):1417–1425
48. Moulin E, Assaad J, Delebarre C (2000) Modeling of Lamb waves generated by integrated transducers in composite plates using a coupled finite element-normal modes expansion method. J Acoust Soc Am 107(1):87
49. Muller DE (1956) A method for solving algebraic equations using an automatic computer. Math Tables and Other Aids to Comput 10(56):208–215
50. Nelson R, Dong S (1973) High frequency vibrations and waves in laminated orthotropic plates. J Sound Vib 30(1):33–44
51. Piersol A, Paez T (2009) Harris's shock and vibration handbook, 6th edn. McGraw-Hill Professional, New York
52. Royer D, Dieulesaint E (2000) Elastic waves in solids I: free and guided propagation. Springer, Berlin
53. Ryue J, Thompson D, White P, Thompson D (2009) Decay rates of propagating waves in railway tracks at high frequencies. J Sound Vib 320:955–976
54. Terrien N, Osmont D, Royer D, Lepoutre F, Déom A (2007) A combined finite element and modal decomposition method to study the interaction of Lamb modes with micro-defects. Ultrasonics 46:74–88
55. Tian J, Gabbert U, Berger H, Su X (2004) Lamb wave interaction with delaminations in CFRP laminates. Comput Mater Continua 1(4):327–336
56. Trefethen LM (2000) Spectral Methods in MATLAB. SIAM, Philadelphia
57. Velichko A, Wilcox P (2007) Modeling the excitation of guided waves in generally anisotropic multilayered media. J Acoust Soc Am 121(1):60–69
58. Vivar-Perez JM (2012) Analytical and Spectral Methods for the Simulation of Elastic Waves in Thin Plates. VDI Fortschritt-Berichte Reihe 20 Nr. 441

59. Vivar Perez JM, Ahmad ZAB, Gabbert U (2013) Membrane carrier wave function in the modelling of Lamb wave propagation. CEAS Aeronaut J 4:51–59
60. Vivar Perez JM, Duczek S, Gabbert U (2014) Analytical and higher order finite element hybrid approaches for an efficient simulation of ultrasonic guided waves I: 2D-analysis. Smart Struct Syst 13:587–614
61. von Ende S, Schäfer I, Lammering R (2007) Lamb wave excitation with piezoelectric wafers – an analytical approach. Acta Mech 193(3–4):141–150
62. Wilcox P (2004) Modeling the excitation of Lamb and SH waves by point and line sources. AIP Conf Proc 700:206–213
63. Willberg C, Vivar Perez JM, Duczek S, Ahmad ZAB (2015) Simulation methods for guided-wave based structural health monitoring: A review. Appl Mech Rev 67:1–20
64. Yang J (2005) An introduction to the theory of piezoelectricity. Advances in mechanics and mathematics, vol 9. Springer, Berlin
65. Zheng-Sheng Y, Yao-Zhi C, Min-Jae O, Tae-Wan K, Qun-Sheng P (2006) An efficient method for tracing planar implicit curves. J Zheijang Univ Sci A 7(7):1115–1123
66. Zienkiewicz OC, Taylor RL (2000) The finite element method: volume 1 the basis. Butterworth Heinemann, Oxford